Quaternary Research

doi:10.1017/qua.2019.45

East Asian winter monsoon evolution since the late Pliocene based on a pollen record from Lake Xingkai, northeast Asia

Shouzhen Xin[a,b]*, Ji Shen[a,b]*, Wenfang Zhang[a], Weiwei Sun[a], Xiayun Xiao[a]

[a]State Key Laboratory of Lake Science and Environment, Nanjing Institute of Geography and Limnology, Chinese Academy of Sciences, Nanjing 210008, China
[b]University of Chinese Academy of Sciences, Beijing 100049, China
*Corresponding authors at: Nanjing Institute of Geography and Limnology, Chinese Academy of Sciences, 73 East Beijing Road, Nanjing 210008, China.
E-mail addresses: xinshzh@126.com (S. Xin); jishen@niglas.ac.cn (J. Shen).

(Received November 24, 2018; Accepted June 28, 2019)

Abstract

A 328.58 m drill core (XK12) was recovered from lacustrine–alluvial sediments in the Xingkai Basin, northeast China, with the aim of obtaining a high-resolution pollen record of East Asian winter monsoon (EAWM) evolution since 3.6 Ma. An index based on the pollen record of thermophilous trees and terrestrial herbs is used as an indicator of winter temperature conditions controlled by the EAWM, at the glacial–interglacial scale. Primary age control was established based on lithostratigraphy and magnetostratigraphy, and then the pollen index was correlated to the LR04 global benthic $\delta^{18}O$ record and finally tuned to Earth orbital obliquity to produce a high-resolution astronomical time scale. The pollen record indicates that the EAWM underwent two stepwise enhancements at 2.8 and 1.6 Ma. These events are consistent with paleoclimatic records of mean quartz grain size from the Chinese Loess Plateau, and they are also in accord with the initiation and intensification of Northern Hemisphere glaciation. Our findings suggest that the variability of the EAWM since 3.6 Ma was primarily controlled by changes in global ice volume and climatic cooling.

Keywords: East Asian winter monsoon; Lake Xingkai; Pollen record; Pliocene; Pleistocene; Astronomical time scale

INTRODUCTION

As an integral part of the global climate system, the Asian monsoon system provides heat and precipitation that directly affect the livelihood of nearly half of the world's population. Thus, knowledge of their spatiotemporal variation is essential for decision making and management in the context of sustainable development (WCRP, 2009; Wang et al., 2014b; An et al., 2015). The East Asian monsoon, a unique subtropical–extratropical monsoon system that can extend poleward to ~50°N latitude, has been established since at least the early Miocene (Sun and Wang, 2005; Guo et al., 2008). As one half of the East Asian monsoon, the East Asian winter monsoon (EAWM) was initiated by the development of the Siberian high, and it transmits high-latitude climate signals to subtropical and tropical regions, resulting in a strong cold and dry northerly circulation over East Asia, thereby affecting a quarter of the Northern Hemisphere (Liu, 1985; Chang, 2004; Wang et al., 2017).

Since the 1990s, the evolution of the EAWM since the Pliocene, on both tectonic and orbital time scales, has been reconstructed using proxy indicators from the Chinese Loess Plateau and the South China Sea (mainly drill cores obtained during ODP Leg 184) (Fig. 1a). Records of grain size distributions and dust flux of the windblown loess-paleosol and red clay sections in the Chinese Loess Plateau are usually used to reconstruct the variability of the EAWM (Liu and Ding, 1993; Ding et al., 1994, 1995, 2002; Lu et al., 2000). In addition, the mean grain size of quartz particles (MGSQ) in loess-paleosol and red clay sequences has been recognized as a reliable proxy for reconstructing variations in EAWM intensity, due to the stability of quartz during post-depositional modification, weathering, and pedogenesis, as well as its relatively stable provenance (Xiao et al., 1995; Sun et al., 2000, 2006b; Amit et al., 2014). Several geochemical indicators with high sensitivity to weathering and pedogenesis, such as the Zr/Rb ratio and Sr and Nd isotopes, have also been used to reconstruct EAWM variations (Liu et al., 2004; Chen et al., 2006; Wang et al., 2007). Both the

Cite this article: Xin, S., Shen, J., Zhang, W., Sun, W., Xiao, X. 2020. East Asian winter monsoon evolution since the late Pliocene based on a pollen record from Lake Xingkai, northeast Asia. *Quaternary Research* 93, 40–59. https://doi.org/10.1017/qua.2019.45

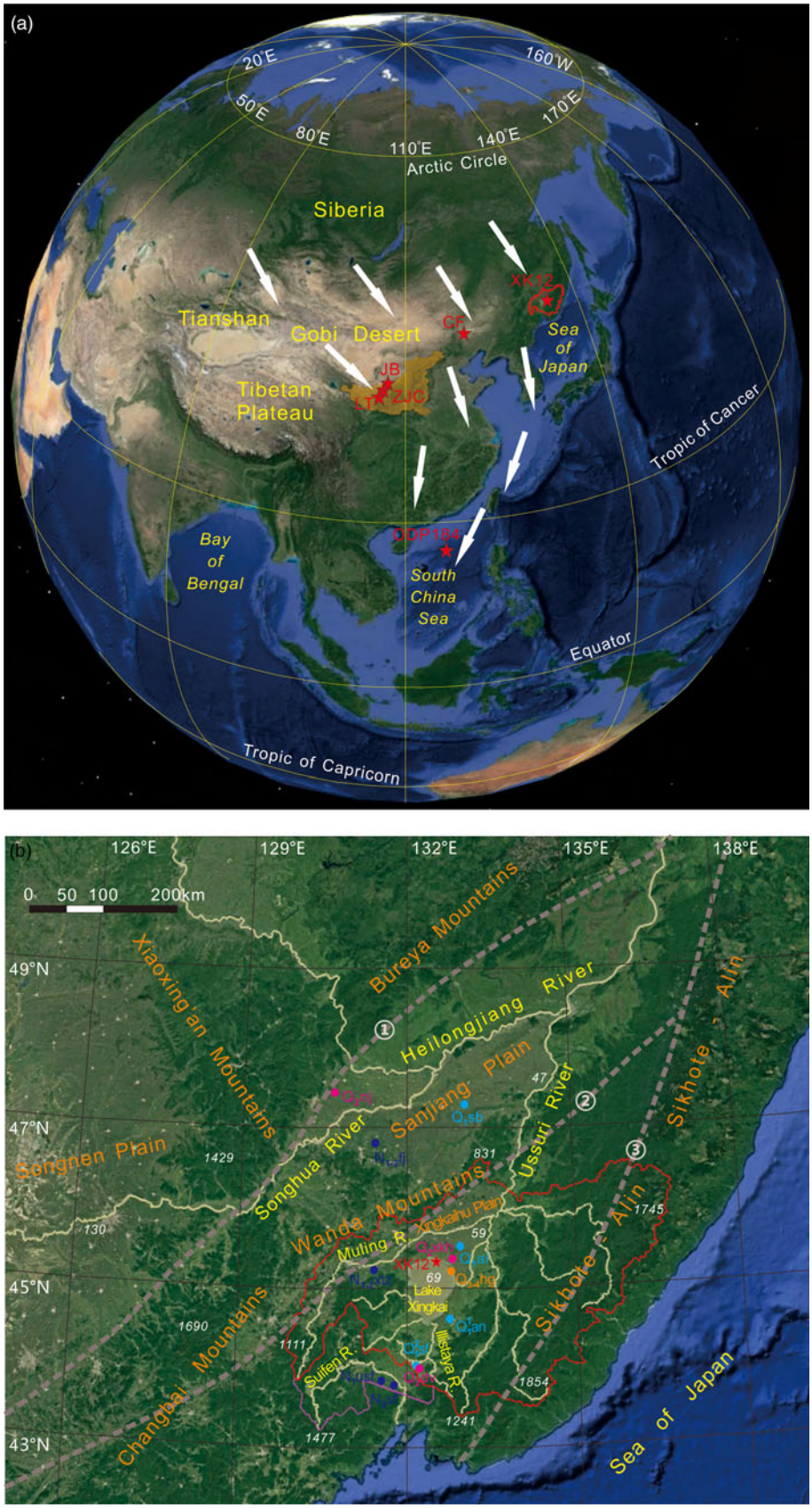

Figure 1. (a) Location of Xingkai Basin (the area enclosed by the red line), loess sections (JB, Jingbian section; ZJC, Zhaojiachuan section; LT, Lingtai section; CF, loess sections near Chifeng City, Inner Mongolia), and marine sediment cores drilled during Ocean Drilling Program Leg 184. Orange shading indicates the Chinese Loess Plateau; white arrows indicate East Asian winter monsoon trajectories and extent. The

https://doi.org/10.1017/qua.2019.45 Published online by Cambridge University Press

strength and duration of the EAWM increased during glacial periods, which resulted in enhanced upwelling and mixing that supplied increased quantities of nutrients to the surface of the East Asian marginal seas. Therefore, enhanced biological productivity during glaciations is revealed by various proxies from the northern South China Sea (Tian et al., 2005; Wan et al., 2007; Zhao et al., 2009). In the northern South China Sea, records of clay minerals (Wan et al., 2007) and planktonic foraminifera (Li et al., 2004) from ODP Site 1146 have revealed enhancement of the EAWM between 3.1 and 2 Ma.

Variations of the East Asian monsoon since the late Pliocene are closely linked to global glacial–interglacial cycles, and therefore proxies of East Asian monsoon intensity from the Chinese Loess Plateau have been correlated to the global marine $\delta^{18}O$ record to provide a chronostratigraphic framework (Liu, 1985; Kukla et al., 1988; Maher and Thompson, 1992; Liu and Ding, 1993). Orbital parameters, especially obliquity, which influences summer insolation in high-latitude regions, drive global ice volume fluctuations and have been recognized as the predominant forcing factor of changes in the EAWM (Liu and Ding, 1993, 1998; Ding et al., 2002; Sun et al., 2006a). In addition, a low-latitude EAWM record based on surface and subsurface temperature differences in the northern South China Sea indicated that the mean state of the super El Niño–Southern Oscillation strongly modulated EAWM variability during 2.8–1.2 Ma, while the intensity of Northern Hemisphere glaciation (NHG) was not sufficient to dominate EAWM variations; this changed after 0.9 Ma (Li et al., 2017). Various driving mechanisms of the EAWM have been inferred from records from different domains of the monsoon region. A high-resolution EAWM record spanning the late Neogene from elsewhere in East Asia is needed to clarify the interactions between EAWM variations and other components of the global climate system, especially in northeast Asia, where the climate is directly affected by the EAWM.

Well-preserved long-term terrestrial paleoenvironmental archives are scarce in northeast Asia. Loess deposits surrounding the Horqin and Otindag Deserts in Chifeng, northeast China, have been used to reconstruct the climatic evolution of the region since ~1.22 Ma (Zeng et al., 2016) (Fig. 1a). In addition, thick sequences of alluvial and lacustrine deposits have accumulated in the sedimentary basins of northeast Asia, and sedimentary sections of different ages can be used to reconstruct East Asian monsoon behavior. Fossil plant remains of Calabrian age preserved in the Pavlovskoe brown coal field in the Russian Far East are characterized by taxonomic diversity. Studies using multiple techniques have been conducted on various paleobotanical organ types and have revealed the effects of the East Asian monsoon on the climate of the region during the last 200 ka of the Calabrian (Bondarenko et al., 2013). Cenozoic continental deposits are well exposed in open cast mines used for brown coal exploitation in basins in the southern part of the Russian Far East. Analysis of 14 different floral horizons has been conducted in order to reconstruct climate change during intervals from the middle Eocene to the early Pleistocene (Utescher et al., 2015). Unfortunately, however, no long, continuous record has yet been obtained of the evolution of the East Asian monsoon in high-latitude northeast Asia.

Xingkai Basin is located in northeast Asia and is directly influenced by the Siberian high that promotes the equatorward development of a strong EAWM (Sun et al., 2018) (Fig. 1). It has subsided substantially since its initial formation in the early Cenozoic (Korotkii et al., 2007), which has favored the preservation of a continuous, rapidly accumulated sedimentary sequence well suited for reconstructing the evolution and variability of the EAWM. In this study, we present pollen, lithostratigraphic, and paleomagnetic evidence from a 328.58-m-long core of lacustrine–alluvial sediments drilled in the Xingkai Basin. We use the results to reconstruct the evolution of the EAWM since the Pliocene, with the aim of providing new insights into its forcing mechanisms.

STUDY AREA

Xingkai Basin, in the upper and middle reaches of the Ussuri River, is the southernmost part of the Heilongjiang (Amur) River system and has an area of ~105,000 km^2. Xingkaihu Plain, comprising about one fifth of the area, is a flat alluvial–lacustrine plain located in the north of the basin. Xingkaihu Plain is surrounded by mountains: the Sikhote-Alin to the east, the Wanda Mountains to the north, and the Changbai Mountains to the west. Lake Xingkai (Khanka) is a major tributary of the Ussuri River, located in the southwest part of Xingkaihu Plain. The surface area is 4200 km^2, the catchment area is ~20,400 km^2, the average water depth is ~4.5 m, the maximum water depth is ~10 m, and the elevation of the modern lake level is 69 m above sea level (m asl) (Long et al., 2015; Sun et al., 2018). The only outflow is the Songacha River in the eastern part of the lake basin (Fig. 1).

Figure 1. (Continued) base maps is from Google Earth. Figure 1. **(b)** The location of drilling core XK12 and stratotypes mentioned in the text. The area enclosed by the red line is the Xingkai Basin, and the area enclosed by the purple line is the middle and upper reaches of the Suifen River. Gray dashed lines are fault belts: 1, Jiamusi-Yitong fault belt; 2, Fushun-Mishan fault belt; 3, middle Sikhote-Alin fault belt. The red star is the location of drilling core XK12, and blue dots are the locations of Neogene stratotypes. N_1usf, Ust-Suifunskaya Fm.; N_2sf, Shufanskaya Fm.; N_{1-2}xlz, Xialiangzi Fm.; N_{1-2}fj, Fujin Fm. Cyan dots indicate the locations of lower Pleistocene stratotypes. Q_1^1an, Annenskaya Fm.; Q_1^2sf, Suifunskaya Fm.; Q_1al, alluvial sediment member in Xingkaihu Plain; Q_1sb, Suibin Fm. Magenta dots are locations of middle Pleistocene stratotypes. Q_2nj, Nongjiang Fm.; Q_2xkh, Xingkaihu Fm.; Q_2dv, lacustrine sediment member, which is the dividing range between the Xingkai Basin and the modern Suifen River. The orange dot labeled "Q_{3-4}hg" is the Hugang Fm. The base map is from Google Earth. (For interpretation of the references to color in this figure legend, the reader is referred to the web version of this article.)

https://doi.org/10.1017/qua.2019.45 Published online by Cambridge University Press

Modern climate and vegetation

The modern climate of Xingkai Basin is mainly determined by the East Asian summer and winter monsoon circulation. The annual temperature ranges from 2°C to 5°C, the mean temperature of the warmest month (July) is 22°C, and the mean temperature of the coldest month (January) is about −20°C. Rainfall occurs mainly in summer, with an annual total of ~540 mm (Sun et al., 2018).

The modern vegetation of Xingkai Basin consists of meadows, bogs, and forests in almost equal proportions. Meadows are widespread in the poorly drained parts of Xingkaihu Plain and in the river valleys, and bogs occur in floodplain and lakeshore areas. The main forest type in the lowlands is Mongolian oak (*Quercus mongolica*), forming pure stands or occurring in mixed broadleaf forest with *Populus*, *Betula*, *Ulmus*, and *Fraxinus* (Xia, 1988; Kolbek et al., 2003). Temperate mixed forest occurs on the mountains surrounding Xingkai Basin (40°15′–50°20′N, 126°–135°30′E); it is codominated by *Pinus koraiensis* and various broadleaf trees, including *Quercus*, *Tilia*, *Betula*, *Acer*, *Fraxinus*, *Ulmus*, and *Populus*, together with the heliophilous conifer *Abies holophylla* (only south of 44°N). At 600–800 m asl, the temperate communities may include the boreal dominants *Picea jezoensis*, *Picea koraiensis*, and *Abies nephrolepis* (Sun and Weng, 1992; Ren and Zhang, 1998; Kolbek et al., 2003).

Geology, Neogene and Quaternary stratigraphy

Sanjiang Plain, Xingkaihu Plain, and the upper and middle reaches of the Suifen (Razdol'naya) River, have developed in the uniform structural deformation zone of northeast Asia (Zhang et al., 2015). These three depressions have undergone synchronous tectonic subsidence controlled by faults on their two sides since they came into existence in the early Cenozoic (BGMRHP, 1993; Pavlyutkin and Petrenko, 2010). As a result of river capture in the middle Pleistocene, the modern Suifen River turns to the south near Ussuriysk and flows into the Sea of Japan. Before this, the path of the paleo-Suifen River turned to the northeast to the north of Ussuriysk and crossed the modern dividing range between the middle reach of the Suifen River and Xingkai Basin, and then flowed into the Xingkai Basin, which made it an important tributary of Lake Xingkai (Belyanina et al., 2009; Bondarenko et al., 2013). Thus, the Ussuri River once linked the three depressions to form an integrated river system. The upper and middle reaches of the Suifen River and the mountainous areas around Xingkai Basin that are the source of modern tributaries comprised the upper reach of the Ussuri River before the middle Pleistocene. Tributaries flowed into the flat Xingkaihu Plain, and some of them merged to form a lake that constitutes the middle reach of the Ussuri River. The lower reach of the Ussuri River starts from Raohe canyon between the Xingkaihu and Sanjiang Plains and ends where the Ussuri River joins the Heilongjiang River in Sanjiang Plain. Before the middle Pleistocene, these three interconnected depressions synchronously accumulated sediments and underwent erosional deformation; thus, the regional strata of these depressions can potentially be correlated in detail. In addition, as a result of geologic surveys and mining activity over several decades in northeast China and the Russian Far East, late Cenozoic sedimentary stratotypes in the southern part of northeast Asia continent are well established (Figs. 1b and 2).

The widespread Neogene system in the middle reach of the Suifen River mainly comprises the Ust-Suifunskaya and Shufanskaya Formations (Fm.), both consisting of alluvial–lacustrine sediments and basalt. The Ust-Suifunskaya Fm., which extends to the south of Xingkai Basin and the middle reach of the Suifen River, is mainly of late Miocene age and is characterized by the occurrence of the pollen of *Fagus* (Pavlutkin and Petrenko, 2010). The Shufanskaya Fm. developed within the middle reach of the Suifen River and has an unconformable contact with the underlying Ust-Suifunskaya Fm., which is mainly of Pliocene age. Pollen assemblages in the upper part of the formation are dominated by *Pinus* and *Betula*, with the rare occurrence of *Juglans*, *Quercus*, *Fagus*, *Acer*, and *Tilia*. The increasing representation of cold-tolerant forest at the expense of thermophilous trees likely reflects substantial major climatic cooling at the beginning of the Pleistocene. In addition, the upper basalt horizon of the formation has a reversed magnetic polarity and is likely derived from a volcanic eruption in the early Matuyama chron (Pavlutkin and Petrenko, 2010) (Figs. 1b and 2). This evidence indicates that Neogene alluvial–lacustrine sedimentation in the middle reach of the Suifen River continued until the end of the Pliocene.

The Xialiangzi Fm. is widely distributed in Xingkaihu Plain and consists mainly of Neogene alluvial–lacustrine sediments. The stratotype of the Xialiangzi Fm. formed in the western branch of Xingkaihu Plain (the Muling River valley), where the formation is relatively thin compared with the depocenters of the plain, and contains interbedded basalt derived from volcanic eruptions of the nearby Changbai Mountains. In the central Xingkaihu Plain, this formation is buried by Quaternary deposits, and in the western mountainous area, it is covered by the Jidong Basalt (dated to 3.36–4.09 Ma by the K-Ar method, as is the case for basalt ages referenced herein) (BGMRHP, 1993) (Figs. 1b and 2). The Fujin Fm. is the Neogene stratotype of Sanjiang Plain. This alluvial–lacustrine stratum can generally be divided into two parts: the bottom part begins with lacustrine clay and silty sand and ends with coal-bearing siltstone; and the top part is greenish-gray to gray sand, silty sand, and clay. These two Neogene formations in both the Xingkaihu and Sanjiang Plains are dated to the Miocene through Pliocene, and their pollen flora is dominated by angiosperms (BGMRHP, 1993) (Figs. 1b and 2). Comparison of the Neogene stratotypes from the three depressions linked by the paleo-Suifen River reveals the occurrence of thin sedimentary deposits in the upper reach valley, interbedded with basalt lava; and thick and continuous sedimentary deposits in the middle and lower reaches, with the absence of basalt lava. There is generally an unconformity between the Neogene

https://doi.org/10.1017/qua.2019.45 Published online by Cambridge University Press

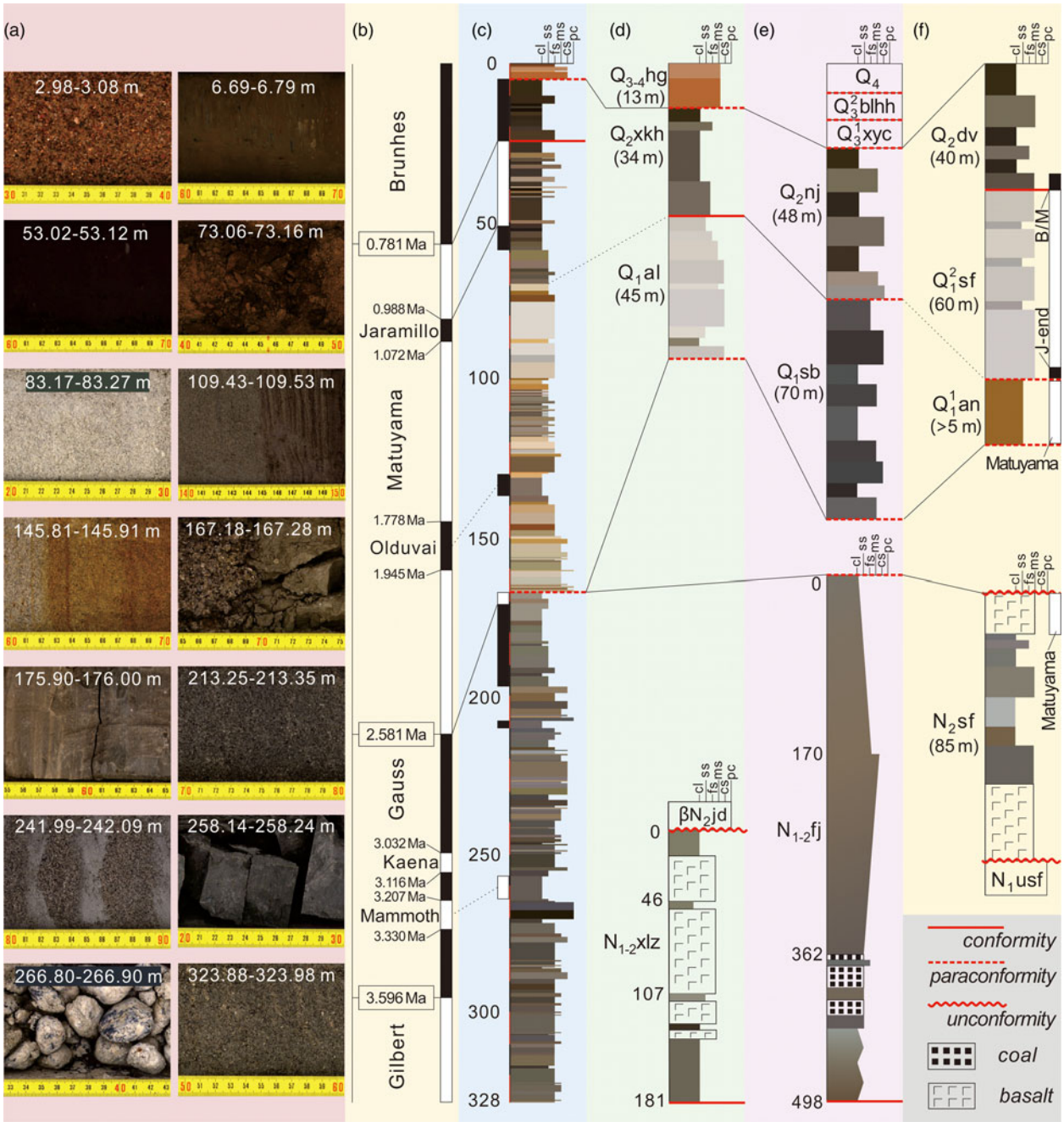

Figure 2. (color online) Photos of selected intervals from core XK12 (a). Standard paleomagnetic polarity column with ages (Ogg, 2012) (b). Lithostratigraphy and geomagnetic polarity column of core XK12 (c). Correlation of Neogene–Quaternary stratotypes in Xingkaihu Plain (d), Sanjiang Plain (e), and the middle reach of the paleo-Suifen River (f). The labels of stratotypes are mainly given in the caption for Fig. 1b. Other labels: $\beta N_2 jd$, Jidong Basalt; Q_3^1 xyc, Xiangyangchuan Fm.; Q_3^2 blhh, Bielahonghe Fm.; Q4, Holocene sediments. Lithologic labels: cl, clays; ss, silt sand; fs, fine sand; ms, medium sand; cs, coarse sand; pc, pebble and cobble.

alluvial–lacustrine strata and the overlying Pleistocene deposits. Deposition continued until the very end of the Pliocene, even in the upper reach of the Ussuri River.

The Quaternary system is widely developed across the whole of the three depressions and consists of mainly alluvial and lacustrine deposits. The stratigraphic contact between the Quaternary and underlying strata is a parallel unconformity. In the middle and lower reaches of the Ussuri River, namely the Xingkaihu and Sanjiang Plains, respectively, the lower Pleistocene deposits range from poorly sorted diluvial to alluvial sands and lacustrine silts and clays. The strata in Sanjiang Plain are usually thicker than those in Xingkaihu Plain. There is a fining upward of the grain size, and the thickness of the strata gradually decreases from the center to the margin of the basins. The early Pleistocene alluvial–lacustrine strata in Xingkaihu Plain are characterized by light-colored, poorly

https://doi.org/10.1017/qua.2019.45 Published online by Cambridge University Press

rounded vein quartz detritus. The Suibin Fm., deposited in Sanjiang Plain in the early Pleistocene, is enriched in dark-colored detritus with occasional interbeds of silt and clay. Following the termination of the deposition of the Suibin Fm., there was a transient uplift event in Sanjiang Plain, resulting in a partial paraconformity with the overlying middle Pleistocene deposits. This paraconformity horizon has been defined as the boundary between the lower and the middle Pleistocene in the Sanjiang and Xingkaihu Plains and is dated to 1.2 Ma, slightly earlier than the beginning of the Jaramillo geomagnetic event. After 1.2 Ma, the Xingkaihu Fm. and Nongjiang Fm. were deposited in the Xingkaihu and Sanjiang Plains, respectively. These two sequences of middle Pleistocene lacustrine sediments are homogeneous in lithology, which indicates the occurrence of a major stage of lake development within these two depressions during the Quaternary (BGMRHP, 1993; Qi et al., 2015) (Figs. 1b and 2).

In the middle reach of the Suifen River and the upper reach of the Ussuri River, the lower Pleistocene consists of two sections. The Annenskaya Fm. is characterized by brownish-red lacustrine sand and clay layers and is widespread within the southern part of Xingkai Basin; in the southern part of Xingkaihu Plain, it is overlain by early Pleistocene greenish-gray sands and clays. Its provenance is a variously colored piedmont weathering crust developed along the slopes around the southern Xingkai Basin. The Annenskaya Fm. is characterized mainly by reversed geomagnetic polarity, and therefore its age corresponds to the beginning of the Matuyama chron, that is, the Gelasian stage (Pavlutkin and Petrenko, 2010) (Figs. 1b and 2). The overlying Suifunskaya Fm. occurs in the middle reach of the Suifen River and farther north in Xingkaihu Plain. This formation has a clear erosional unconformity with the underlying Annenskaya Fm. The Suifunskaya Fm. consists of alluvial sand and pebbles derived from acidic light-colored vein quartz with notable amounts of granite and andesite debris. Based on pollen assemblages, this formation is of early Pleistocene age, possibly extending into the early stage of the middle Pleistocene (Pavlutkin and Petrenko, 2010) (Figs. 1b and 2). A recent paleomagnetic study of the Suifunskaya Fm. constrained its age to the interval between the Jaramillo and the Brunhes/Matuyama (B/M) boundary (Bondarenko et al., 2013). Above the Suifunskaya Fm., dark gray clays and fine sand are present with a conformable contact. This lacustrine sedimentary sequence in the middle reach of the Suifen River and southern Xingkai Basin is considered to be of middle Pleistocene age.

In summary, before 1.2 Ma, when alluvial sediments began to be widely deposited in the Xingkaihu and Sanjiang Plains (i.e., in the middle and lower reaches of the Ussuri River, respectively), proximal sediments began to be intermittently deposited in the middle reach of the Suifen River (i.e., the upper valley of the Ussuri River). After 1.2 Ma, continuous deposition of lacustrine sediments started in the Xingkaihu and Sanjiang Plains, while the middle reach of the Suifen River started to accumulate alluvial deposits. After the B/M boundary, continuous accumulation of lacustrine sediments with identical color and lithologic characteristics began in all three depressions. This homogeneous lacustrine sedimentation represents the principal stage of lake development in the Ussuri River catchment during the Quaternary. However, shortly afterward, lacustrine sedimentation ceased abruptly and almost simultaneously. The unconformity on the top of the widespread lacustrine strata marks the termination of middle Pleistocene sedimentation throughout the entire Ussuri River catchment, and subsequently no sizable stable sedimentary environment existed in the middle and lower reaches of the Ussuri River.

In the late Pleistocene, two series of terraces formed together with Lake Xingkai and major rivers in the Sanjiang and Xingkaihu plains. Terrace II, named the Xiangyangchuan Fm., formed in the early stage of the late Pleistocene; and terrace I, named the Bielahonghe Fm., formed in the late stage of the late Pleistocene. The sediments in floodplains, marshland, and paleochannels comprise the major part of the Holocene series in the Sanjiang and Xingkaihu Plains (BGMRHP, 1993). Notably, the northern margin of paleo-Lake Xingkai is delimited by four prominent sand ridges on the broad coastal plain; they are interpreted as representing four distinct periods of lake lowstand that caused beach exposure and provided a more extended sand source for foredune formation around Lake Xingkai (Qiu et al., 1988; Long and Shen, 2015). The sandy ridges are mainly composed of well-sorted brown to brownish-red eolian sand with distinct cross-bedding structures, and are defined as the late Pleistocene and Holocene series, termed the Hugang Fm. (BGMRHP, 1993; Long and Shen, 2015) (Figs. 1b and 2). The Suifen River was separated from the upper reach of the Ussuri River in the middle Pleistocene (Bondarenko et al., 2013), which was likely the result of neotectonic activity and river capture, and subsequently the middle Pleistocene lacustrine strata acted as a dividing range between them.

MATERIALS AND METHODS

Drill core XK12

Core XK12 (45°18′48.90″N, 132°34′57.40″E, 75 m asl) was drilled on the sandy beach ridge of the northern lakeshore (Fig. 1). The use of internal plastic tubing during drilling minimized twisting and distortion of the core (Shen et al., 2010). The total depth of the core is 328.58 m, with a recovery of up to 90.8%.

The sedimentary sequence recovered in core XK12 can be divided into three parts, including two normal sedimentary cycles. The top 0–5.10 m consists of brown, brownish-red, and rusty well-sorted and well-rounded eolian sands with distinct cross-bedding structures. The middle part, 5.10–167.23 m is a normal sedimentary cycle. The lacustrine interval ranges from 5.10 to 59.15 m and consists of dark clays and silty sand, with thin interbeds of fine sand. The interval from 59.15 to 149.61 m is mainly alluvial sediments; from 75.60 to 99.75 m, is homogeneous light-colored fine sand; and the remaining strata are mainly variously colored fine and silty sands. Notably, the interval of 129.81–136.85 m is

https://doi.org/10.1017/qua.2019.45 Published online by Cambridge University Press

a clay deposit, and the lower part from 149.61 to 167.23 m consists of diluvial deposits of poorly sorted light-gray coarse sand with a silty matrix and occasional pebbles. The bottom part, 167.23–328.58 m consists of another normal sedimentary cycle. The top interval, 167.23–197.09 m, consists of gray to greenish-gray lacustrine clays and silty sand; the middle interval, from 197.09 to 270.57 m, consists of diluvial and alluvial layers, with clay layers from 207.90 to 210.28 m and 257.11 to 264.25 m, and a riverbed pebble and cobble horizon at 265.30–270.57 m. The remaining interval, 270.57–328.58 m, is gray to greenish-gray medium sand with a relatively uniform color and lithology (Fig. 2).

Pollen analysis

A total of 1164 pollen samples were collected at an average interval of 20 cm in the upper 200 m, and at an average interval of 40 cm in the lower part. The samples were processed following standard procedures (Moore et al., 1991): approximately 1–2 g of sediment was digested with 10% HCl and 40% HF to remove carbonate and SiO_2, respectively, after which the sample was passed through a 7 μm mesh sieve. Tablets containing a known quantity of *Lycopodium* spores were added to each sample to determine pollen concentrations. Pollen identification and counting were performed using a Leitz optical microscope. The analyses were completed at Zihua Biotechnology in Shijiazhuang, China. The results are expressed as both percentages and concentrations. The pollen percentages of terrestrial plants (trees, shrubs, and herbs) were calculated based on a sum of terrestrial pollen, while the percentages of aquatics, fern spores, and algae are based on the sum of total pollen and spores. The pollen percentage diagram of selected pollen taxa and genera was plotted using Tilia Software (Grimm, 2011). The zonation of pollen assemblages was defined to six zones (1–6) using the constrained incremental sum-of-squares cluster analysis (CONISS) (Grimm, 1987) based on the stratigraphic distributions of all the encountered pollen taxa, with 1, 4 and 6 subdivided into three distinct subzones (Supplementary Fig. S1).

Paleomagnetic measurements

A total of 1321 orientated cubic samples (2 × 2 × 2 cm) were selected at intervals of 10–30 cm from core XK12 for paleomagnetic measurements. Magnetizations were measured using a 2G-755R cryogenic superconducting magnetometer housed in a magnetically shielded space (<150 nT) at the Institute of Earth Environment, Chinese Academy of Sciences. All samples were progressively demagnetized at fields up to 80 mT at 2–10 mT increments. Alternating-field demagnetization results were evaluated using orthogonal vector endpoint projection (Zijderveld, 1967). The vector directions of the characteristic remanent magnetization (ChRM) component were calculated using principal components analysis (Kirschvink, 1980), in which the ChRM component passes through the origin and is defined by a minimum of four consecutive demagnetization steps. ChRM components with a maximum angular deviation (MAD) >15° or absolute inclination >70° or <20° were rejected. A total of 379 samples produced valid demagnetization results. The results are presented in Supplementary Table S1, the orthogonal vector endpoint projection and intensity evolution plots for demagnetization of representative samples are presented in Supplementary Fig. S2. The vector directions determined from the ChRM directions were used to define a geomagnetic polarity sequence. Only the results from five continuous intervals of clay-rich sediments were used to construct the magnetostratigraphy; this was because of the possibility of loose sandy sediments being disturbed during drilling, core splitting, and sampling. In addition, there were limited data available from core sections with a high sand content (Fig. 3).

RESULTS

Lithostratigraphic correlation

Xingkaihu Plain was directly linked with Sanjiang Plain and the Suifen River catchment as a result of the development of the Ussuri River system. Since their formation, the subsidence and deformation of these three depressions has been controlled by fault belts belonging to a uniform tectonic system. Therefore, their sedimentary strata are readily correlated, which provides the basis for establishing an initial chronostratigraphic framework for core XK12.

Core XK12 was drilled on a sandy beach ridge that constitutes the northern shore of modern Lake Xingkai. The top 5.10 m belongs to the Hugang Fm., characterized by bright-colored and well-sorted eolian sands with well-rounded grains. This section can be divided into the Dahugang and Taiyanggang horizons at the top and bottom, respectively (BGMRHP, 1993) (Fig. 2). Radiocarbon dates from human bones from an ancient tomb excavated in Dahugang (ATHP, 1979) and optically stimulated luminescence dating results from Taiyanggang (Qiu et al., 2007) indicate that this part of core XK12 is of late Pleistocene to Holocene age. There is a distinct paraconformity between the eolian deposit and the underlying lacustrine sediments.

Dark-gray lacustrine clays and silty sand are continuously present below 5.10 m. The paraconformity horizon at the top of the lacustrine sediments can be correlated with the top of the middle Pleistocene Xingkaihu Fm. and the Nongjiang Fm. and with the surface of the dividing range between the Xingkai Basin and the Suifen River catchment. The paleomagnetic results reveal a transition from normal to reversed polarity at 25.00 m. Because the B/M boundary between dark-gray lacustrine sediments and the light-colored Suifunskaya Fm. marks the boundary between the early and middle Pleistocene, we assign the interval of 5.10–25.00 m of core XK12 to the middle Pleistocene (Fig. 2).

According to the paleomagnetic results of the upper lacustrine section, the end boundary of the Jaramillo event occurs at a depth of 51.40 m. The base of the lacustrine section at 59.15 m corresponds approximately to the bottom of the Suifunskaya Fm. in the middle reach of the Suifen River,

https://doi.org/10.1017/qua.2019.45 Published online by Cambridge University Press

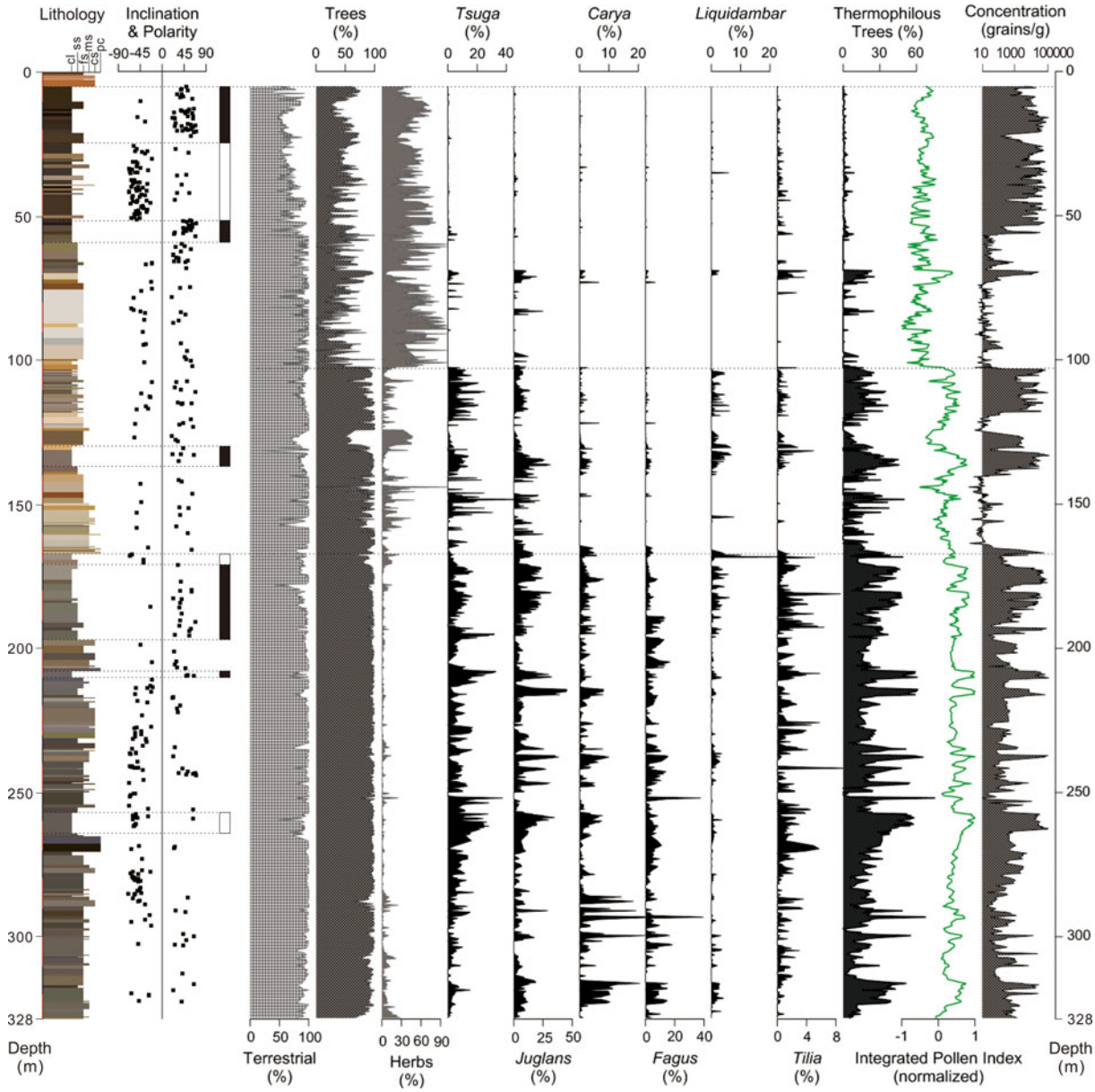

Figure 3. Lithology, paleomagnetic polarity sequence, pollen spectra diagram, and integrated pollen index (green curve) for core XK12. (For interpretation of the references to color in this figure legend, the reader is referred to the web version of this article.)

which corresponds approximately to the beginning of the Jaramillo event. The alluvial and diluvial sands within the interval of 75.60–167.23 m are coeval with early Pleistocene alluvial deposits in Xingkaihu Plain and the Suibin Fm. in Sanjiang Plain. The lower variously colored sediments are likely equivalent to the Annenskaya Fm. in the upper reach of the Ussuri River. The interval of lacustrine sediments from 129.81 to 136.85 m, with a normal polarity, may have been deposited during the Olduvai event. Therefore, the pronounced paraconformity at 167.23 m in core XK12 can be determined to be the base of the Quaternary (Fig. 2).

Although there are no continuous long-term Neogene stratotypes established in Xingkai Basin, the Shufanskaya Fm. in the middle reach of the Suifen River provides comparable information about sedimentation at the end of the Pliocene (Pavlutkin and Petrenko, 2010). The upper basalt horizon of the Shufanskaya Fm. has a reversed geomagnetic polarity and is derived from a volcanic eruption at the beginning of the Matuyama chron. The underlying lacustrine horizon would have been deposited not much earlier than the end of the Pliocene. The three depressions were closely linked by the development of the Ussuri River system, and consequently, the lacustrine horizon deposited in the middle reach of the Suifen River (upper reach of the Ussuri River) can be correlated with the lacustrine horizons in the middle and lower reaches of the Ussuri River. Thus, we propose that this lacustrine horizon of the Shufanskaya Fm. can be correlated with the interval of lacustrine sediments from 167.23 to 197.09 m in core XK12 and also with the top part of the Fujin Fm. in Sanjiang Plain. Therefore, the lower normal sedimentary

https://doi.org/10.1017/qua.2019.45 Published online by Cambridge University Press

cycle in core XK12 continued until the end of the Pliocene. Furthermore, the paleomagnetic results for this lacustrine part of core XK12 reveal a transition from normal to reversed polarity at 170.90 m, which is probably the Matuyama/Gauss (M/G) boundary (Figs. 2 and 3). From 170.90 m to the bottom of the core, there is a continuous sequence of alluvial and diluvial sands, corresponding to the upper sandy horizon of the Fujin Fm. According to the mean sedimentation rate of ~10 cm/ka estimated for the upper part of core XK12 and the lower Pleistocene series of Sanjiang Plain (Qi et al., 2015), the bottom of core XK12 extends roughly to the boundary between the upper and lower Pliocene. The clay horizon at 207.90–210.28 m has a normal polarity and was likely deposited in the later part of the Gauss chron. The other clay horizon, at 257.11–264.25 m, is of reversed polarity and may correspond to the Kaena or Mammoth events.

Integrated pollen index of the EAWM

Xingkai Basin is a semiclosed basin surrounded by mountains with altitudes of 300–1800 m. Rivers supply sediment including pollen from different altitudes and transport directions (Fig. 1b). Wind dispersal is another agent that transports pollen into the plain and results in pollen mixture within the basin. But pollen transported into the basin by wind might be rare because of the high mountains surrounding the basin. Thus, the pollen assemblages from core XK12 are an integrated record of changes in the vegetational composition of the entire Xingkai Basin. Temperate mixed forest has been the major forest type in the Xingkai Basin since the Oligocene (Pavlyutkin, 2015). The East Asian monsoon system, which has directly influenced the Xingkai Basin, was established in the early Miocene (Guo et al., 2008). Most of the plant taxa in the region are temperature sensitive and therefore would be strongly affected by the intensity of EAWM, which is an important determinant of whether temperate plants can survive the winter (Bondarenko et al., 2017; Lyu et al., 2018).

Although many plant taxa responded to changes in EAWM intensity, the thermophilous trees (*Tsuga*, *Fagus*, *Carya*, *Juglans*, *Liquidambar*, *Tilia*) were the most sensitive to changes in EAWM intensity, and their pollen records exhibit the largest variations in amplitude. In addition, the latitude of the Xingkai Basin corresponds roughly to their northern distribution limit in the Holocene (Fang et al., 2011). Despite the large climatic fluctuations since the Pliocene, these thermophilous trees underwent limited evolutionary changes in terms of their climatic tolerance (Svenning, 2003; Bondarenko et al., 2017); their response to warm and cold climatic shifts was to migrate northward and southward, respectively. Therefore, we assume that variations in the percentages of the pollen of the thermophilous trees in core XK12 can be used as a sensitive indicator of fluctuations in EAWM intensity since the Pliocene. Notably, since the early Pleistocene, increases in the percentages of terrestrial herbs occurred at the expense of the thermophilous trees. This is likely because thermophilous trees expanded into habitats also suitable for terrestrial herbs during interglacial intervals, and it was only when the thermophilous trees decreased or disappeared in glacial intervals that terrestrial herbs were able to expand in response to the decreased forest density. Thus, variations in the percentages of both of these vegetational components were closely linked to climate changes. The zone boundaries at ~100 and ~167 m identified by CONISS indicate the major transitions of the percentages of the six thermophilous tree genera and of the terrestrial herb taxa (Fig. 3).

The pollen percentages of the six thermophilous tree genera exhibit a common pattern of fluctuations throughout the core; in addition, as expected, the sum of terrestrial herb taxa shows an inverse pattern of variation with the thermophilous trees (Fig. 3). The sum of these two groups was normalized to zero mean and unit variance. The two records were then summed and smoothed with a 3-point running mean, and the result was then normalized (Fig. 3). The range of the sum of the taxa in the two groups was similar, and therefore they were not weighted. Notably, the index represents on average more than 37% of the total terrestrial pollen, and it provides an efficient summary of the major vegetational and climatic changes in the Xingkai Basin. Low values indicate strong winter frost conditions (i.e. an intensified EAWM), and vice versa (Figs. 3 and 4).

Astronomically tuned time scale

The evolution of the EAWM on the glacial–interglacial time scale was mainly driven by ice sheet variations (Liu and Ding, 1993; Ding et al., 2002; Sun et al., 2006a), which are reflected by the LR04 stacked benthic $\delta^{18}O$ record (Lisiecki and Raymo, 2005). The integrated pollen index from core XK12, which is regarded as an EAWM indicator and therefore influenced by variations in global ice volume, would be expected to show a pattern of fluctuations similar to that of the marine $\delta^{18}O$ record. The resolution of the chronostratigraphic framework established by stratigraphic correlation and magnetostratigraphy is too low to investigate the evolution of the EAWM on the glacial–interglacial time scale. Therefore, we developed an astronomically tuned time scale based on the high-resolution integrated pollen index. Matching paleoclimatic records to time series of orbital parameters (i.e., orbital tuning) has proven useful for developing age models and has been widely applied to marine sediments (Raymo et al., 1989; Ruddiman et al., 1989; Shackleton et al., 1990; Hilgen, 1991a, 1991b; Tian et al., 2002; Palike et al., 2006; Ao et al., 2011; Yi et al., 2018), Chinese loess-paleosol and red clay sequences (Ding et al., 1994, 2002; Lu et al., 1999; Heslop et al., 2000; Sun et al., 2006a), and continental lacustrine and fluvial strata (Prokopenko et al., 2006; Hu et al., 2007; Ao et al., 2012; Nowaczyk et al., 2013; Torres et al., 2013).

The following steps were followed to produce a tuned age model for core XK12. First, three magnetostratigraphic age control points (the B/M boundary at 25.0 m, the end of the Jaramillo event at 51.4 m, and the M/G boundary at 170.9 m) were selected to establish an initial age model (Ogg,

https://doi.org/10.1017/qua.2019.45 Published online by Cambridge University Press

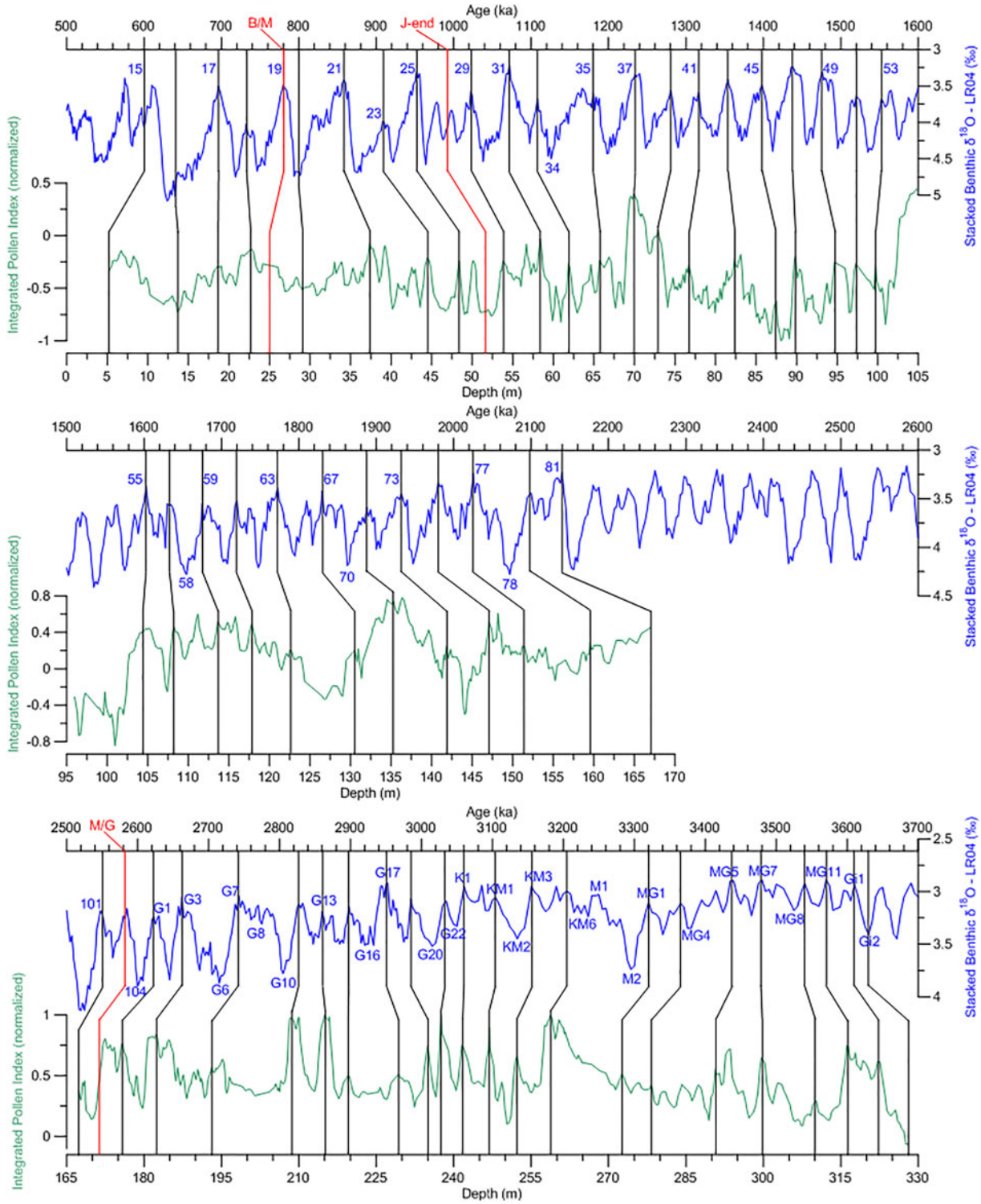

Figure 4. Initial age model for core XK12. Results of the visual correlation of the integrated pollen index (green) from core XK12 with the LR04 benthic $\delta^{18}O$ stack (blue) (Lisiecki and Raymo, 2005). The three red lines are independent geomagnetic age control points. (For interpretation of the references to color in this figure legend, the reader is referred to the web version of this article.)

2012) (Figs. 2 and 4). This model was fixed during the subsequent tuning processes. As expected, the fluctuations and phase of the integrated pollen index were very similar to the variations of the LR04 $\delta^{18}O$ stack (Lisiecki and Raymo, 2005) (Fig. 4). Then, assuming a direct relationship between global ice volume fluctuations and EAWM intensity, we visually correlated the integrated pollen index from core XK12 to the LR04 curve. Peaks in the integrated pollen index were correlated with troughs in the LR04 stack, representing interglacial stages; and troughs in the integrated pollen index were

https://doi.org/10.1017/qua.2019.45 Published online by Cambridge University Press

correlated to peaks in the LR04 stack, representing glacial stages (Fig. 4). Fifty-eight age control points were thereby obtained, and they are listed in Supplementary Table S2 and Fig. 4. The resulting average sediment accumulation rate of the section between the B/M boundary and the end of the Jaramillo event is 12.75 cm/ka. Notably, the sediment accumulation in Sanjiang Plain in the early and middle Pleistocene was estimated to be 10 cm/ka (Qi et al., 2015).

Next, a suitable target curve was selected to establish an astronomical time scale. The La2004 astronomical solution computed with present-day input values for the dynamical ellipticity of the Earth and tidal dissipation in the evolution of the Earth–Moon system (Laskar et al., 2004) has been shown to be appropriate for geologic records (Palike et al., 2006; Husing et al., 2007). The obliquity parameter has been suggested to have a stronger and more consistent influence on climate change since the Pliocene than either precession or eccentricity (Ruddiman et al., 1986; Muller and MacDonald, 1997; Huybers, 2006; Tian et al., 2008; Naish et al., 2009). Both the LR04 stack and Chinese loess records exhibit distinct fluctuations at a frequency corresponding to that of obliquity in the late Pliocene and early Pleistocene (Ding et al., 1994; Lisiecki and Raymo, 2005). Thus, the orbital obliquity curve of La2004 was selected as the target curve for astronomical tuning. The time scale of the LR04 stack is based on the assumption that the ice sheets were directly modulated by orbital variations (Imbrie and Imbrie, 1980; Lisiecki and Raymo, 2005), and therefore when conducting the visual correlation, the initial age model would have incorporated the lag inherent in the LR04 stack. Therefore, during the tuning process, we assumed zero lag between calculated obliquity and the obliquity signal in the integrated pollen index record of core XK12.

Because of the sedimentary hiatus in core XK12 in the early Pleistocene, the tuned time scale of core XK12 was developed separately in two parts. The dynamic optimization method (Yu and Ding, 1998) was used to filter the obliquity (41 ka) signal from the integrated pollen index based on the initial age model, and then the filtered curve was compared with the orbital obliquity curve. This process was repeated multiple times, slightly altering the age control points of the initial age model to achieve a satisfactory correlation. The most plausible result is illustrated in Fig. 5. At the end of this iterative tuning procedure, we selected 35 and 23 age control points to establish an astronomically tuned time scale for the Pleistocene and Pliocene sections, respectively. The initial and final age control points are listed in Supplementary Table S2, and the integrated pollen index with astronomically tuned ages is listed in Supplementary Table S3.

During the tuning, a constant sedimentation rate was assumed between two adjacent age control points. The age control points remained at a fixed depth from the initial age model, and the age difference before and after the tuning of each point was no more than 10 ka (see Supplementary Table S2). This tuning procedure resulted in better correlations between filtered obliquity and orbital obliquity and between the integrated pollen index and the LR04 stack. Another important constraint on tuning was that the sediment accumulation rate should not change abruptly (Sun et al., 2006a). According to the tuned time scale of core XK12, the sediment accumulation rate was relatively uniform, ranging from 5 to 25 cm/ka. After tuning, the ages of the top and the bottom of the Pliocene section of core XK12 are 2.54 and 3.63 Ma, respectively, and the ages of the top and the bottom of the Pleistocene section are 0.60 and 2.15 Ma, respectively (Fig. 5).

DISCUSSION

Influence of neotectonic activity on the regional sedimentary environment

In northeast Asia, tectonic activity and the associated fault zones have determined the distribution of sedimentary basins and the surrounding mountains (Ding, 1988). Although major basins such as the Sanjiang and Xingkaihu Plains subsided and were subject to almost continuous sediment accumulation during the late Cenozoic, sedimentary hiatuses caused by intermittent neotectonic activity, accompanied by volcanic eruptions and changes in river systems, have occurred (Korotkii et al., 2007; Qiu et al., 2014). There are many paraconformities and unconformities in the Neogene and Quaternary stratotypes in northeast Asia (Fig. 2). The widespread stratigraphic evidence shows that sedimentary hiatuses exist and are possibly related to neotectonic activity. Stratigraphic correlation has revealed two paraconformities in core XK12: one in between the topmost eolian Hugang Fm. and the middle Pleistocene lacustrine clays, and the other in between the early Pleistocene diluvial sands and Neogene lacustrine clays (Figs. 2 and 4). This indicates that the graben depression of Xingkaihu Plain was affected at least twice by intermittent regional tectonic activity since the late Pliocene. The high-resolution astronomically tuned time scale for core XK12 provides further information about the causes and processes of these interruptions in sedimentation.

The late Pliocene interval of core XK12 and the Fujin Fm. consists mainly of alluvial sands interbedded with diluvial material. These very thick deposits with comparable lithology and color indicate that the Sanjiang and Xingkaihu Plains experienced a long stage of fluvial development during 3.63–2.76 Ma. Alluvial sedimentation likely accompanied continuous differential tectonic activity, mountain uplift was the source of coarse clastic material, and basin subsidence provided accommodation space for sedimentation. The late Pliocene Jidong Basalt and the lower basaltic part of the Shufanskaya Fm. confirm the occurrence of synchronous tectonic activity in the adjacent Changbai Mountains (BGMRHP, 1993; Pavlutkin and Petrenko, 2010) (Fig. 2). After 2.76 Ma, lacustrine sediments began to be deposited in Xingkaihu Plain, which was synchronous with the development of the Fujin Fm., and even with the silt and clay sediments of the middle part of the Shufanskaya Fm. This indicates that the Ussuri River catchment commenced a

https://doi.org/10.1017/qua.2019.45 Published online by Cambridge University Press

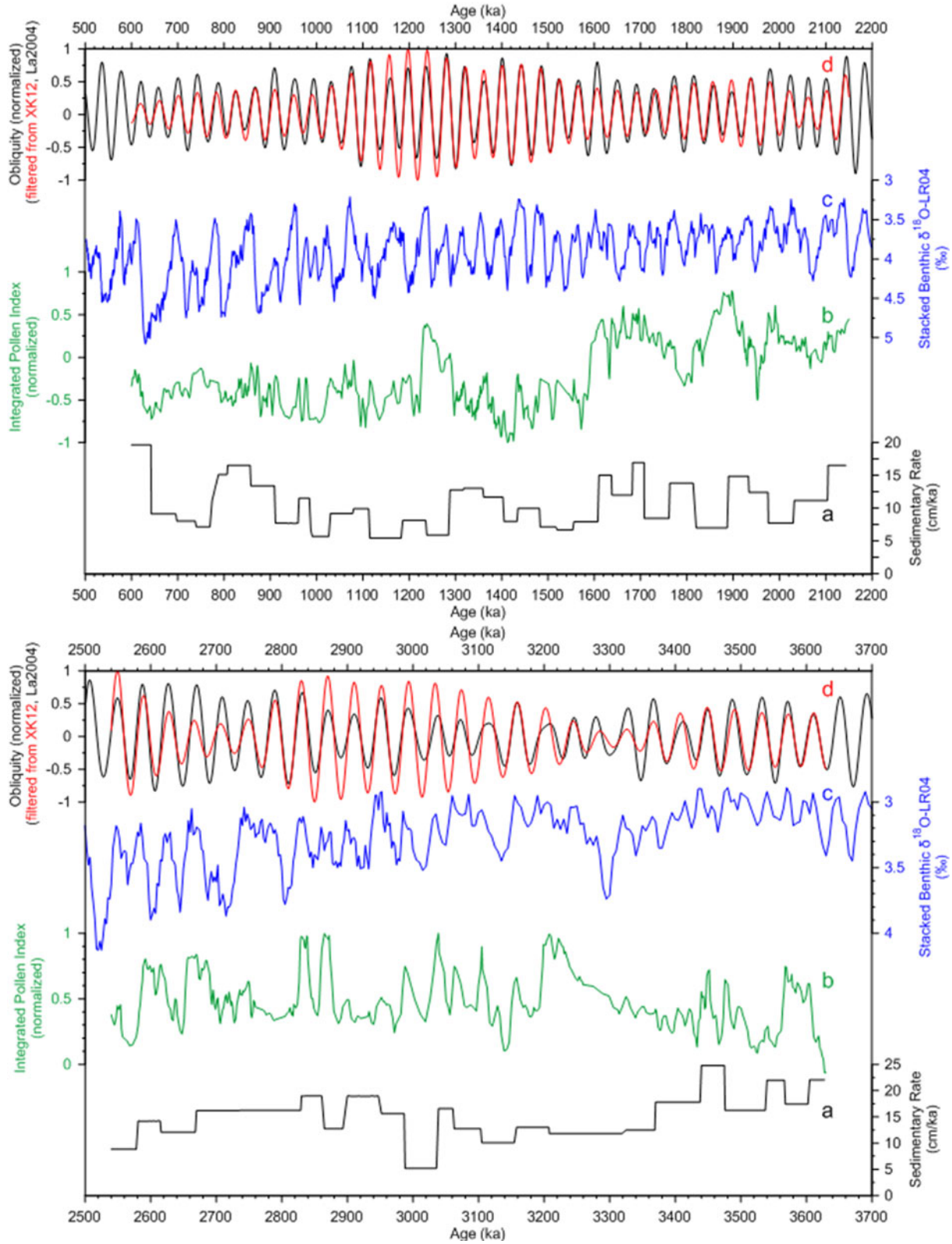

Figure 5. Astronomically tuned time scale for core XK12: (a) sedimentation rate of core XK12; (b) integrated pollen index of core XK12; (c) LR04 benthic $\delta^{18}O$ stack (Lisiecki and Raymo, 2005); and (d) comparison of filtered obliquity curve from the integrated pollen index (red) and calculated orbital obliquity (black) (Laskar et al., 2004). (For interpretation of the references to color in this figure legend, the reader is referred to the web version of this article.)

https://doi.org/10.1017/qua.2019.45 Published online by Cambridge University Press

phase of steady subsidence. The development of the river system was accompanied by the formation of large lakes in the middle and lower reaches of the Ussuri River.

At the beginning of the Pleistocene, at 2.54 Ma, lacustrine sedimentation at the site of core XK12 and in Sanjiang Plain ceased abruptly, and at the same time a volcanic eruption resulted in the deposition of basalt overlying the lacustrine sediments of the Shufanskaya Fm. in the middle reach of the Suifen River. This widespread paraconformity serves as the isochronal Neogene/Quaternary boundary in northeast Asia (BGMRHP, 1993; Pavlutkin and Petrenko, 2010) (Fig. 2) and was most likely the result of major regional tectonic activity. The uplift of the entire basin induced rapid fluvial incision, when watercourses cut into the loose sedimentary deposits. These major geomorphological changes reduced the ability of local sedimentary archives to record environmental changes. A volcanic episode occurred in northeast China at around the Pliocene–Pleistocene transition and is represented by the eruption of the Junjianshan Basalt (2.4–2.6 Ma), the lower Jingpohu Basalt (2.4–2.6 Ma), and the Baijin Basalt (2.41 Ma) in Changbai Mountains. Farther north, the uplift of Xiaoxing'an Mountains accompanied the eruption of the Daxiongshan Basalt, which began at 2.5 Ma (Liu, 1987, 1988; BGMRHP, 1993). This tectonic activity and associated volcanism resulted in major modification of the Heilongjiang River system and the disappearance of paleolakes such as Dalianhe-Xiangshun paleolake in the western part of Sanjiang Plain (Qiu et al., 2014). As a direct result of tectonic uplift, the denudation rate in the Heilongjiang River catchment increased substantially during the late Pliocene–Pleistocene (Nicholson et al., 2016). This series of major hydrologic and geomorphic changes substantially altered the sedimentary environment throughout the entire Heilongjiang River catchment and resulted in the widespread paraconformity between the Neogene and Quaternary series.

Subsequently, tectonic uplift weakened and was eventually replaced by subsidence. Sediments began to be deposited in watercourses and then on floodplains and terraces, finally infilling the valleys created by the previous uplift. This process developed retrogressively, from the lower reaches and then to the middle and upper reaches, in sequence. Sediment deposition at the site of core XK12 recommenced at 2.15 Ma. First, poorly sorted diluvial sediments were deposited, probably soon after the accumulation of the Suibin Fm. in Sanjiang Plain. The diluvial sediments in core XK12 are variously colored and differ substantially from those of the Suibin Fm., but they are similar to those of the Annenskaya Fm. in the southern part of the Xingkai Basin. The provenance of the diluvial sediments is the variously colored weathering crust developed along the slopes around the southern and western parts of the Xingkai Basin. During this period, the different reaches of the Ussuri River were characterized by diverse sedimentary environments. Alternating alluvial and lacustrine sedimentation in Sanjiang Plain indicates the development of a fluvial–lacustrine system. The diluvial sediments in core XK12 indicate geomorphic differences in Xingkaihu Plain, and the altitudinal difference between the Xingkaihu and Sanjiang Plains was also substantial. The thin, proximal lacustrine Annenskaya Fm. with a paraconformity at its surface indicates that a small, transient lake likely developed in the upper Ussuri River valley. Eventually, a sequence of light-colored alluvial sands was deposited at the site of core XK12, which clearly correspond to the lower Pleistocene alluvial sediments in Xingkaihu Plain and the middle Pleistocene Suifunskaya Fm. in the middle reach of the Suifen River (Fig. 2). This diachronous sedimentary horizon was likely caused by the combination of a uniform provenance and a developing fluvial system.

At 1.2 Ma, a paraconformity developed in places between the Suibin and Nongjiang Fms. (Fig. 2), which may have been caused by transient tectonic uplift in northeast Asia. The Longgang volcanic episode in northeast China occurred during 0.8–1.5 Ma, represented by basaltic eruptions in the Mudanjiang River valley (0.89–1.39 Ma) and in Longgang Mountain (0.86–1.23 Ma) of the Changbai Mountains (Liu, 1987, 1988). Subsequently, the altitudinal difference between the Xingkaihu and Sanjiang Plains decreased; lacustrine sedimentation began to occur in Xingkaihu Plain, and light-colored alluvial sediments began to be continuously deposited in the middle reach of the Suifen River. This sedimentary environmental evolution of the Heilongjiang River catchment is also recorded by the appearance of paleo-Lake Songliao in the upper reach (Zhan et al., 2019). Following the B/M geomagnetic polarity transition, all three depressions of the Ussuri River began to accumulate dark-gray lacustrine sediments that represent the main stage of regional lake development in the Quaternary. According to the record of core XK12 and other stratotypes in the Ussuri River catchment, diluvial, alluvial, and lacustrine sedimentation occurred in sequence, indicating steady subsidence of Xingkaihu Plain during 2.15–0.60 Ma.

At 0.60 Ma, lacustrine sedimentation in the three depressions ceased abruptly and almost synchronously. This likely resulted from intense regional tectonic activity related to the Baitoushan volcanic episode in the Changbai Mountains, which started at ~0.58 Ma (Liu, 1987, 1988). In the southern Xingkai Basin, part of the alluvial–lacustrine planation surface began to be uplifted and became the dividing range between the modern Xingkai Basin and the Suifen River catchment (Belyanina et al., 2009; Bondarenko et al., 2013). Farther west, the Songliao dividing ranges were uplifted in the middle of Songliao Plain (Qiu et al., 2014). This type of general regional uplift, together with large-scale falls in sea level as a result of the increased amplitude of glacial–interglacial climate fluctuation, promoted headward erosion in the river valleys of northeast Asia. These geomorphic, hydrologic, and climatic factors together resulted in the successive disappearance of a series of paleolakes that had previously developed in northeast Asia, including paleo-Lake Songliao (Qiu et al., 2014; Zhan et al., 2019).

After the abrupt end of sedimentation in 0.60 Ma, the failure of the Xingkaihu and Sanjiang Plains to accumulate sediments reflects the occurrence of only weak and partial subsidence. In the late Pleistocene, the previously deposited

https://doi.org/10.1017/qua.2019.45 Published online by Cambridge University Press

sediments underwent fluvial incision, and two series of terraces and wide floodplains formed within the valleys of large rivers (BGMRHP, 1993). Four conspicuous sand ridges, representing four distinct periods of lake lowstand, formed in the northern margin of Lake Xingkai (Qiu et al., 1988; Long et al., 2015). However, the flat surface of the plains remained almost intact, including the lacustrine dividing range between the Xingkai Basin and the Suifen River. These low erosion rates were likely due to the low relative elevation difference between the dividing range and the valleys on the two sides and the low absolute altitudes of the entire Heilongjiang and Ussuri River catchments. Thus, the whole of northeast Asia entered a phase of tectonic quiescence following the previous rapid uplift phase.

Evaluation of the astronomical time scale

We now address the robustness of the astronomical time scale of core XK12 from three perspectives. First, all of the major tributaries of the Xingkai Basin are sourced from mountains in the east and southwest, which are occupied by coniferous and mixed broadleaf–coniferous forest at higher elevations. The rivers then flow through areas dominated by broadleaf forest in the piedmont zones, and then through meadow and peatland in the lowlands, before finally discharging into the plain (Fig. 1b). Therefore, the pollen record preserved in the lacustrine sediments of Xingkaihu Plain likely reflects the integrated vegetational history of the entire basin. In addition, Xingkaihu Plain is very flat, resulting in frequent river channel migration. Continuous lateral erosion by the large tributaries would have resulted in the mixing of new alluvial sediments with previously deposited sediments on the surface of the plain. Therefore, most of the alluvial sediment sequences in the plain would have preserved a pollen record that reflected integrated vegetational conditions across the entire basin rather than solely within the plain. In addition, it is difficult for old pollen to be incorporated into newly deposited sediments due to the progressive subsidence of the sedimentary basin. Consequently, the lacustrine and alluvial sediments preserved in Xingkaihu Plain can provide a reliable record of the history of the entire Xingkai Basin on millennial through orbital time scales.

Second, reference to the ages of geomagnetic polarity reversal boundaries is an effective means of evaluating the astronomical time scale. The ages of the three geomagnetic polarity reversals selected to establish an initial age model were fixed during the entire tuning process. The astronomically tuned age of the early Pleistocene interval of clay sediments in core XK12 from 129.81 to 136.85 m is 1.815 to 1.900 Ma; this interval is of normal polarity and corresponds to the Olduvai subchron. The astronomically tuned age of the Pliocene interval of clay sediments from 207.90 to 210.28 m is 2.827 to 2.840 Ma; this interval is of normal polarity and falls within the Gauss chron. The other Pliocene interval of clay sediments, from 257.11 to 264.25 m, has an astronomically tuned age of 3.195 to 3.255 Ma; there are two reversed geomagnetic events within this interval, each with a duration of more than 60 ka. If this section is considered to record the Mammoth event, then an error of at least 25 ka error exists in the astronomically tuned time scale; and if it is considered to be part of the Kaena event, then the error is at least 145 ka (Ogg, 2012) (Fig. 2).

In addition, a layer of well-sorted and well-rounded pebbles and cobbles is present at 265.30–270.57 m in core XK12, which reflects fluvial incision by the river and continuous subsidence of the plain. Notably, the lithology and color of the sediments above and below the pebble layer are uniform. This distinctive sedimentary sequence is quite different to that which would result from regional tectonic uplift (Fig. 2), and therefore the formation of this riverbed horizon can be attributed to a rapid fall in the base level of the lower reaches of the Heilongjiang River. Considering that both the altitude and elevation range of the Heilongjiang River system are quite small, we assume that sea-level change was the cause of the rapid fall in base level. Notably, the tuned age of the riverbed horizon is 3.263–3.308 Ma, corresponding to Marine Isotope Stage (MIS) M2 (Lisiecki and Raymo, 2005) (Figs. 5 and 6). MIS M2 is characterized by the largest increase in benthic $\delta^{18}O$ value in the late Pliocene, indicating a major fall of global sea level (Dwyer and Chandler, 2009; Miller et al., 2012). This fall of global sea level may have triggered worldwide headward erosion, including of the Heilongjiang River system. As a result, the Xingkai Basin would have been scoured due to the resulting headward erosion of the Ussuri River, and the site of core XK12, which was previously a depocenter, would have been subjected to fluvial incision. This fluvial incision event occurred against a background of continuous basin subsidence, which would have promoted the deposition of the thick layer of fluvial pebbles and cobbles at the site of core XK12. After MIS M2, alluvial sedimentation recommenced in Xingkaihu Plain. As mentioned earlier, river channel migration occurs frequently in a flat, subsiding plain. After a brief period of alluvial sedimentation, the main stream moved away from the site of core XK12, and an oxbow lake formed. The interval of clay-rich sediments from 257.11 to 264.25 m in core XK12 likely represents deposition within such a lake. Thus, this interval, which is of reversed polarity, can be confirmed as being deposited within the Mammoth event rather than during the later Kaena event (Fig. 2).

From the foregoing, we conclude that the geomagnetic evidence confirms the reliability of the astronomical age model of core XK12. Although relatively short sedimentary hiatuses may still occur within the intervals of alluvial and diluvial sediments, the age model for core XK12 can be used to explore regional climatic and environmental changes on the orbital time scale.

Evolution of the EAWM since 3.6 Ma

Based on the integrated pollen index of core XK12 and the astronomical time scale, we now attempt to reconstruct the history of the EAWM since the late Pliocene. To aid interpretation, we compared the record from the Xingkai Basin with

https://doi.org/10.1017/qua.2019.45 Published online by Cambridge University Press

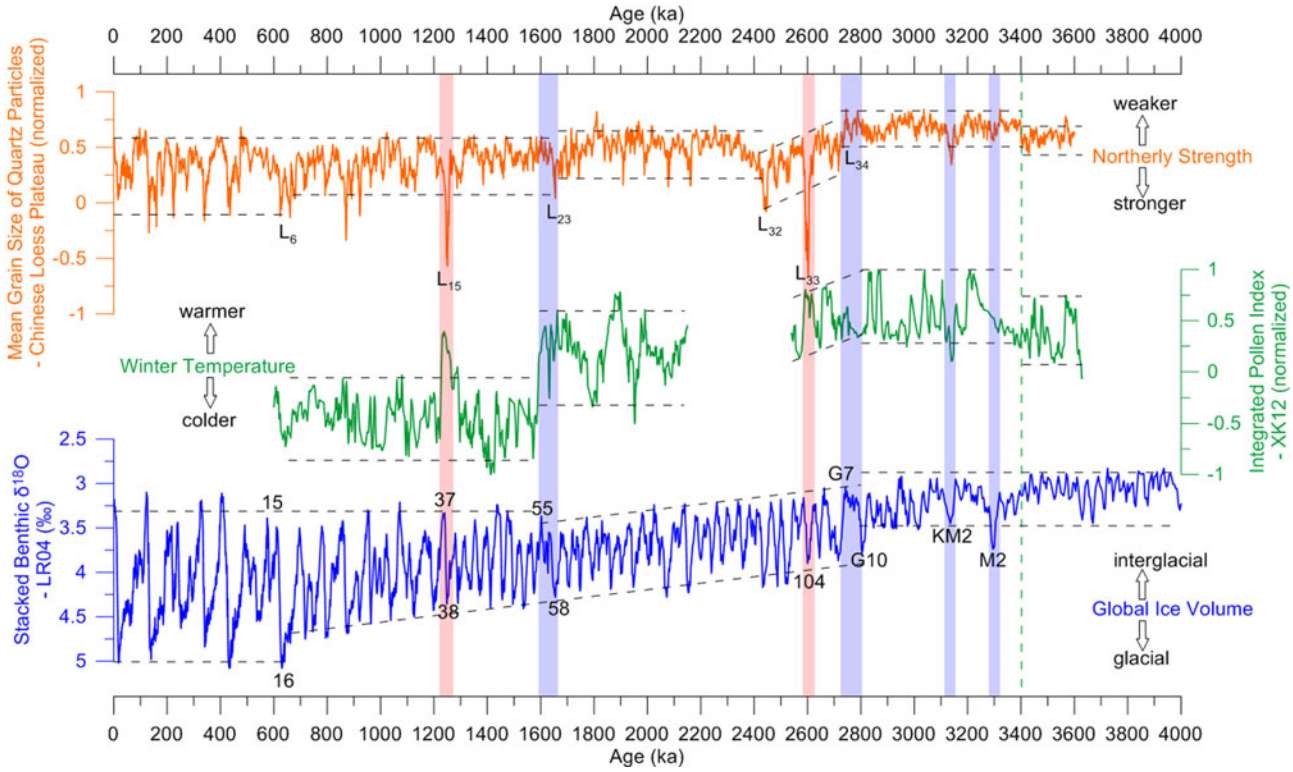

Figure 6. (color online) Comparison of the evolution of the East Asian winter monsoon based on the integrated pollen index of core XK12with the LR04 benthic $\delta^{18}O$ stack (Lisiecki and Raymo, 2005) and stacked mean grain size of quartz particles record from the Lingtai and Zhaojiachuan sections in the Chinese Loess Plateau (Sun et al., 2006a).

paleoclimatic records from the Chinese Loess Plateau and elsewhere. The stacked record of MGSQ, an EAWM proxy, from the Lingtai and Zhaojiachuan sections in the north-central Chinese Loess Plateau (Sun et al., 2006a), was selected for comparison. Except for the Pleistocene hiatuses in core XK12, the integrated pollen index and the MGSQ stack co-vary synchronously, reflecting the stepwise enhancement of the EAWM since 3.6 Ma (Figs. 1a and 6). Comparison of the integrated pollen index, the MGSQ stack, and the LR04 benthic $\delta^{18}O$ stack (Lisiecki and Raymo, 2005) reveals that both the integrated pollen index and the MGSQ stack co-vary with long-term global cooling since 3.6 Ma, with the amplitude of glacial–interglacial fluctuations exhibiting a stepwise increase (Fig. 6).

In the late Pliocene, both records of the EAWM indicate a period of weak winter monsoon beginning at ~3.4 Ma, in the middle Pliocene warm period. The evolution of the EAWM has been used as an indicator of variations in the NHG because of the direct relationship between the two. MIS M2 is identified as representing a major global sea-level fall caused by the initiation of the NHG (De Schepper et al., 2014; Dolan et al., 2015; Tan et al., 2017). Although a layer of riverbed gravel is present in core XK12 in the interval of MIS M2, due to a global sea-level lowstand, the integrated pollen index does not suggest that the EAWM was strong at this time. The MGSQ stack from the Chinese Loess Plateau also fails to indicate a stronger EAWM during MIS M2 (Fig. 6). However, the records from the Xingkai Basin and the Chinese Loess Plateau both reflect an intensified EAWM in the later part of MIS KM2 (Fig. 6). The initiation of the NHG in MIS M2 evidently did not have a substantial effect on the EAWM, possibly indicating that its effects were not globally expressed. Subsequently, in MIS KM2, the intensification of the EAWM may reflect intensified cooling in Siberia, the source area of the EAWM.

The integrated pollen index began to decrease at ~2.8 Ma, during the Pliocene–Pleistocene transition, reflecting the strengthening of the EAWM in the Xingkai Basin (Fig. 6). In addition, there was a continuous coarsening of the MGSQ stack at ~2.72 Ma (Sun et al., 2006a). Before this, on the Chinese Loess Plateau, a typical loess unit, L_{34}, was identified within the uppermost red clay, marking the onset of extensive loess deposition at ~2.8 Ma (Yang and Ding, 2010). Marine isotope records show a major phase of Northern Hemisphere ice sheet growth during 3.3–2.8 Ma (Lisiecki and Raymo, 2005), and a dramatic increase in the supply of ice-rafted debris to the northwest Pacific and the Norwegian Sea at ~2.8 Ma (Maslin et al., 1995). This strengthening of the EAWM over northern China since the late Pliocene indicates a rapid reorganization of the regional climate system in East Asia, which may have been causally related to the initiation of major NHG (Han et al., 1997; Ding et al., 2000; Xiong et al., 2003). In MIS G10 (2.8 Ma), benthic $\delta^{18}O$ values increased to the level of MIS M2 and then increased continuously, indicating a steady increase in NHG (Lisiecki and Raymo, 2005). The trend of EAWM enhancement continued

https://doi.org/10.1017/qua.2019.45 Published online by Cambridge University Press

to the deposition of loess layer L_{32} (2.45 Ma) in the Chinese Loess Plateau (Sun et al., 2006a), and the trend is also evident in the integrated pollen record until the occurrence of a paraconformity in core XK12 at 2.54 Ma (Fig. 6).

In the early Pleistocene, both the integrated pollen index and the MGSQ stack reflect an enhanced EAWM, with fluctuations of larger amplitude than those in the Pliocene. In addition, step-like increases in the EAWM are evident at 1.60 Ma and 1.65 Ma in the Xingkai Basin and the Chinese Loess Plateau, respectively. The climatic event at ~1.6 Ma is recognized in marine records worldwide and has been attributed to the reorganization of oceanic circulation (Lisiecki, 2014; Wang et al., 2014a; Karnauskas et al., 2017). By about MIS 55 (1.6 Ma), the LR04 stack suggests that the maximum global ice volume of interglacial stages reached a limit; however, the volume continued to increase during glacial stages. Consequently, the rate of increase of global ice volume slowed, although the amplitude of glacial–interglacial cycles began to increase at the same time (Lisiecki and Raymo, 2005) (Fig. 6). The difference in timing of the step-like enhancement of the EAWM recorded in the Xingkai Basin and the Chinese Loess Plateau likely reflects regional differences within the EAWM domain of the response to oceanic forcing. It appears that the EAWM intensified first in the middle-latitude Chinese Loess Plateau, and then subsequently at 1.60 Ma in the high-latitude Xingkai Basin.

In the MGSQ stack, the extremely coarse-grained intervals of L_{33} (~2.6 Ma) and L_{15} (~1.25 Ma) are commonly interpreted as representing an unusually strong EAWM (Guo et al., 1998; Ding et al., 2000; Qiang et al., 2001; Sun et al., 2006a, 2010; Zhang et al., 2016). However, no corresponding interval of substantially increased ice volume is evident in the LR04 stack at ~2.6 and ~1.25 Ma, and the integrated pollen index indicates a weak EAWM at these times (Fig. 6). This discrepancy may be the result of genuine regional climatic differences or specific characteristics of the two environmental proxies. It has been proposed that the grain size variations of windblown loess in the Chinese Loess Plateau are controlled by both the distance of the site of deposition to the desert margin (Ding et al., 1999) and the strength of the EAWM (An et al., 1991; Liu and Ding, 1998). A study of three transects across the Chinese Loess Plateau during the last glacial stage showed that extremely coarse loess was only present in the northern part of the plateau and was closely linked to the migration of the southern border of the deserts in northern China, driven by the aridification of the Asian interior. The grain size record of the Jingbian section in the Chinese Loess Plateau indicates four coarsening events at 2.6, 1.2, 0.7, and 0.2 Ma, which were interpreted as reflecting the southward migration of the Mu Us Desert since 3.5 Ma (Ding et al., 2005). In addition, loess began to be deposited at Chifeng, in northeast China, at ~1.22 Ma, which was related to increased inland aridity (Zeng et al., 2016, 2017) (Fig. 1a); furthermore, provenance changes of loess at 2.6 and 1.2 Ma were also related to inland aridification (Ma et al., 2015; Yan et al., 2017). Therefore, we suggest that these two extremely coarse intervals that are evident on the Chinese Loess Plateau might reflect intensified aridity in the Asian interior, and not necessarily the strengthening of the EAWM.

CONCLUSIONS

A 328.58-m-long core of alluvial–lacustrine sediments (XK12) was drilled in Xingkai Basin, northeast Asia, to reconstruct the long-term evolution of the EAWM. The pollen record of thermophilous trees and terrestrial herbs, which is sensitive to winter temperature conditions, was used to produce an index of EAWM variations on the glacial–interglacial time scale. An initial age model was developed based on lithostratigraphy and magnetostratigraphy and was then refined using orbital tuning. The integrated pollen index provides a continuous record of EAWM evolution in northeast Asia since 3.6 Ma, except for two sedimentary hiatuses in the early Pleistocene (2.54–2.15 Ma) and the middle Pleistocene (since 0.60 Ma), which were caused by regional tectonic activities. The integrated pollen index reveals a stepwise pattern of EAWM evolution in the Xingkai Basin, consistent with MGSQ records from the Chinese Loess Plateau. Two major increases in EAWM intensity occurred at ~2.8 and ~1.6 Ma, which are interpreted to reflect the initiation and enhancement of NHG and global cooling.

ACKNOWLEDGMENTS

We thank Professors Youbin Sun and Xiaoke Qiang and Dr. Hao Long for valuable suggestions for the development of the chronology methods. We also thank Dr. Mingming Ma and colleagues for supervising the drilling work, which was conducted by Qinghai Jingcheng Geological & Mining Co., Ltd. We thank Jan Bloemendal for scientific suggestions and for improving the English. Two anonymous reviewers and the editors (Nicholas Lancaster and Wyatt Oswald) are acknowledged for their constructive comments and suggestions, which have greatly improved the article. This work was supported by the National Natural Science Foundation of China (No. 41430530).

SUPPLEMENTARY MATERIAL

To view supplementary material for this article, please visit https://doi.org/10.1017/qua.2019.45.

REFERENCES

Amit, R., Enzel, Y., Mushkin, A., Gillespie, A., Batbaatar, J., Crouvi, O., Vandenberghe, J., An, Z.S., 2014. Linking coarse silt production in Asian sand deserts and Quaternary accretion of the Chinese Loess Plateau. *Geology* 42, 23–26.

An, Z.S., Kukla, G., Porter, S.C., Xiao, J.L., 1991. Late Quaternary dust flow on the Chinese Loess Plateau. *Catena* 18, 125–132.

An, Z.S., Wu, G.X., Li, J.P., Sun, Y.B., Liu, Y.M., Zhou, W.J., Cai, Y.J., *et al*., 2015. Global monsoon dynamics and climate change. *Annual Review of Earth and Planetary Sciences* 43, 29–77.

Ao, H., Dekkers, M.J., Qin, L., Xiao, G.Q., 2011. An updated astronomical timescale for the Plio-Pleistocene deposits from South China Sea and new insights into Asian monsoon evolution. *Quaternary Science Reviews* 30, 1560–1575.

Ao, H., Dekkers, M.J., Xiao, G.Q., Yang, X.Q., Qin, L., Liu, X.D., Qiang, X.K., Chang, H., Zhao, H., 2012. Different orbital rhythms in the Asian summer monsoon records from north and south China during the Pleistocene. *Global and Planetary Change* 80–81, 51–60.

[ATHP] Archaeological Team of Heilongjiang Province, 1979. Excavations at the site of Xingkailiu in Mishan County. [In Chinese with English abstract.] *Acta Archaeologica Sinica* 4, 491–518.

Belyanina, N.I., Belyanin, P.S., Mityureva, E.V., 2009. New evidence for reorientation of the Razdol'naya River flow in the Pleistocene (southern Primor'e region). *Russian Journal of Pacific Geology* 3, 197–200.

Bondarenko, O.V., Blokhina, N.I., Bruch, A.A., Henrot, A.J., Utescher, T., 2017. Quantification of Calabrian vegetation in southern Primory'e (Far East of Russia) using multiple proxies. *Palaeogeography, Palaeoclimatology, Palaeoecology* 467, 253–264.

Bondarenko, O.V., Blokhina, N.I., Utescher, T., 2013. Quantification of Calabrian climate in southern Primory'e, Far East of Russia—an integrative case study using multiple proxies. *Palaeogeography Palaeoclimatology Palaeoecology* 386, 445–458.

[BGMRHP] Burean of Geology and Mineral Resources of Heilongjiang Province, 1993. *Regional Geology of Heilongjiang Province*. [In Chinese with English summary.] Geological Publishing House, Beijing.

Chang, C.P., 2004. *East Asian Monsoon*. World Scientific, Singapore.

Chen, J., Chen, Y., Liu, L.W., Ji, J.F., Balsam, W., Sun, Y.B., Lu, H.Y., 2006. Zr/Rb ratio in the Chinese loess sequences and its implication for changes in the East Asian winter monsoon strength. *Geochimica et Cosmochimica Acta* 70, 1471–1482.

De Schepper, S., Gibbard, P.L., Salzmann, U., Ehlers, J., 2014. A global synthesis of the marine and terrestrial evidence for glaciation during the Pliocene Epoch. *Earth-Science Reviews* 135, 83–102.

Ding, G.Y., 1988. Neotectonic environment, volcanism and deep-seated earthquakes in the northeast China. [In Chinese with English summary.] *Northeastern Seismological Research* 4, 5–11.

Ding, Z., Yu, Z., Rutter, N.W., Liu, T., 1994. Towards an orbital time scale for Chinese loess deposits. *Quaternary Science Reviews* 13, 39–70.

Ding, Z.L., Derbyshire, E., Yang, S.L., Sun, J.M., Liu, T.S., 2005. Stepwise expansion of desert environment across northern China in the past 3.5 Ma and implications for monsoon evolution. *Earth and Planetary Science Letters* 237, 45–55.

Ding, Z.L., Derbyshire, E., Yang, S.L., Yu, Z.W., Xiong, S.F., Liu, T.S., 2002. Stacked 2.6 Ma grain size record from the Chinese loess based on five sections and correlation with the deep sea $\delta^{18}O$ record. *Paleoceanography* 17, 1033–1053.

Ding, Z.L., Liu, T.S., Rutter, N.W., Yu, Z.W., Guo, Z.T., Zhu, R.X., 1995. Ice-volume forcing of East Asian winter monsoon variations in the past 800,000 years. *Quaternary Research* 44, 149–159.

Ding, Z.L., Rutter, N.W., Sun, J.M., Yang, S.L., Liu, T.S., 2000. Re-arrangement of atmospheric circulation at about 2.6 Ma over northern China: evidence from grain size records of loess-palaeosol and red clay sequences. *Quaternary Science Reviews* 19, 547–558.

Ding, Z.L., Sun, J.M., Rutter, N.W., Rokosh, D., Liu, T.S., 1999. Changes in sand content of loess deposits along a north–south transect of the Chinese Loess Plateau and the implications for desert variations. *Quaternary Research* 52, 56–62.

Dolan, A.M., Haywood, A.M., Hunter, S.J., Tindall, J.C., Dowsett, H.J., Hill, D.J., Pickering, S.J., 2015. Modelling the enigmatic late Pliocene glacial event—Marine Isotope Stage M2. *Global and Planetary Change* 128, 47–60.

Dwyer, G.S., Chandler, M.A., 2009. Mid-Pliocene sea level and continental ice volume based on coupled benthic Mg/Ca palaeotemperatures and oxygen isotopes. *Philosophical Transactions of the Royal Society A* 367, 157–168.

Fang, J.Y., Wang, Z.H., Tang, Z.Y., 2011. *Atlas of Woody Plants in China*. Springer, Berlin.

Grimm, E.C., 1987. CONISS: a FORTRAN 77 program for stratigraphically constrained cluster analysis by the method of incremental sum of squares. *Computers & Geosciences* 13, 13–35.

Grimm, E.C., 2011. Tilia 1.7.16 Software. Illinois State Museum, Springfield.

Guo, Z.T., Liu, T.S., Fedoroff, N., Wei, L.Y., Ding, Z.L., Wu, N.Q., Lu, H.Y., Jiang, W.Y., An, Z.S., 1998. Climate extremes in loess of China coupled with the strength of deep-water formation in the North Atlantic. *Global and Planetary Change* 18, 113–128.

Guo, Z.T., Sun, B., Zhang, Z.S., Peng, S.Z., Xiao, G.Q., Ge, J.Y., Hao, Q.Z., *et al*., 2008. A major reorganization of Asian climate by the early Miocene. *Climate of the Past* 4, 153–174.

Han, J., Fyfe, W.S., Longstaffe, F.J., Palmer, H.C., Yan, F.H., Mai, X.S., 1997. Pliocene–Pleistocene climatic change recorded in fluviolacustrine sediments in central China. *Palaeogeography, Palaeoclimatology, Palaeoecology* 135, 27–39.

Heslop, D., Langereis, C.G., Dekkers, M.J., 2000. A new astronomical timescale for the loess deposits of northern China. *Earth and Planetary Science Letters* 184, 125–139.

Hilgen, F.J., 1991a. Astronomical calibration of Gauss to Matuyama sapropels in the Mediterranean and implication for the geomagnetic polarity time scale. *Earth and Planetary Science Letters* 104, 226–244.

Hilgen, F.J., 1991b. Extension of the astronomically calibrated (polarity) time scale to the Miocene/Pliocene boundary. *Earth and Planetary Science Letters* 107, 349–368.

Hu, S., Goddu, S.R., Appel, E., Verosub, K., 2007. Fine-tuning of age integrating magnetostratigraphy, radiocarbon dating, and carbonate cyclicity: example of lacustrine sediments from Heqing Basin (Yunnan, China) covering the past 1 Myr. *Journal of Asian Earth Sciences* 30, 423–432.

Husing, S.K., Hilgen, F.J., Aziz, H.A., Krijgsman, W., 2007. Completing the Neogene geological time scale between 8.5 and 12.5 Ma. *Earth and Planetary Science Letters* 253, 340–358.

Huybers, P., 2006. Early Pleistocene glacial cycles and the integrated summer insolation forcing. *Science* 313, 508–511.

Imbrie, J., Imbrie, J.Z., 1980. Modeling the climatic response to orbital variations. *Science* 207, 943–953.

Karnauskas, K.B., Mittelstaedt, E., Murtugudde, R., 2017. Paleoceanography of the eastern equatorial Pacific over the past 4 million years and the geologic origins of modern Galapagos upwelling. *Earth and Planetary Science Letters* 460, 22–28.

Kirschvink, J.L., 1980. The least-squares line and plane and the analysis of palaeomagnetic data. *Geophysical Journal of the Royal Astronomical Society* 62, 699–718.

https://doi.org/10.1017/qua.2019.45 Published online by Cambridge University Press

Kolbek, J., Srutek, M., Box, E.O., 2003. *Forest Vegetation of Northeast Asia*. Kluwer Academic Publishers, London.

Korotkii, A.M., Grebennikova, T.A., Karaulova, L.P., Belyanina, N.I., 2007. Lacustrine transgressions in the late Cenozoic Ussuri-Khanka depression (Primor'e). *Russian Journal of Pacific Geology* 1, 352–365.

Kukla, G., Heller, F., Ming, L.X., Chun, X.T., Sheng, L.T., Sheng, A.Z., 1988. Pleistocene climates in China dated by magnetic-susceptibility. *Geology* 16, 811–814.

Laskar, J., Robutel, P., Joutel, F., Gastineau, M., Correia, A.C.M., Levrard, B., 2004. A long-term numerical solution for the insolation quantities of the earth. *Astronomy & Astrophysics* 428, 261–285.

Li, B.H., Wang, J.L., Huang, B.Q., Li, Q.Y., Jian, Z.M., Zhao, Q.H., Su, X., Wang, P.X., 2004. South China Sea surface water evolution over the last 12 Myr: a south–north comparison from Ocean Drilling Program sites 1143 and 1146. *Paleoceanography* 19, 1009–1020.

Li, D.W., Zhao, M.X., Tian, J., 2017. Low-high latitude interaction forcing on the evolution of the 400 kyr cycle in East Asian winter monsoon records during the last 2.8 Myr. *Quaternary Science Reviews* 172, 72–82.

Lisiecki, L.E., 2014. Atlantic overturning responses to obliquity and precession over the last 3 Myr. *Paleoceanography* 29, 71–86.

Lisiecki, L.E., Raymo, M.E., 2005. A Pliocene–Pleistocene stack of 57 globally distributed benthic $\delta^{18}O$ records. *Paleoceanography* 20, 1003–1019.

Liu, J.Q., 1987. Study on geochronology of the Cenozoic volcanic rocks in northeast China. [In Chinese with English abstract.] *Acta Petrologica Sinica* 3, 21–31.

Liu, J.Q., 1988. The Cenozoic volcanic episodes in noertheast China. [In Chinese with English abstract.] *Acta Petrologica Sinica* 4, 3–12.

Liu, L.W., Chen, J., Ji, J.F., Chen, Y., 2004. Comparison of paleoclimatic change from Zr/Rb ratios in Chinese loess with marine isotope records over the 2.6–1.2 Ma BP interval. *Geophysical Research Letters* 31, 15204–15207.

Liu, T.S., 1985. *Loess and the Environment*. [In Chinese.] Science Press, Beijing.

Liu, T.S., Ding, Z.L., 1993. Stepwise coupling of monsoon circulations to global ice volume variations during the late Cenozioc. *Global and Planetary Change* 7, 119–130.

Liu, T.S., Ding, Z.L., 1998. Chinese loess and the paleomonsoon. *Annual Review of Earth and Planetary Sciences* 26, 111–145.

Long, H., Shen, J., 2015. Sandy beach ridges from Xingkai Lake (NE Asia): timing and response to palaeoclimate. *Quaternary International* 430, 21–31.

Long, H., Shen, J., Wang, Y., Gao, L., Frechen, M., 2015. High-resolution OSL dating of a late Quaternary sequence from Xingkai Lake (NE Asia): chronological challenge of the "MIS 3a mega-paleolake" hypothesis in China. *Earth and Planetary Science Letters* 428, 281–292.

Lu, H.Y., Liu, X.D., Zhang, F.Q., An, Z.S., Dodson, J., 1999. Astronomical calibration of loess–paleosol deposits at Luochuan, central Chinese Loess Plateau. *Palaeogeography, Palaeoclimatology, Palaeoecology* 154, 237–246.

Lu, H.Y., van Huissteden, K., Zhou, J., Vandenberghe, J., Liu, X.D., An, Z.S., 2000. Variability of East Asian winter monsoon in Quaternary climatic extremes in North China. *Quaternary Research* 54, 321–327.

Lyu, A.Q., Lu, H.Y., Zeng, L., Zhang, H.Y., Zhang, E.L., Yi, S.W., 2018. Vegetation variation of loess deposits in the southeastern Inner Mongolia, NE China over the past similar to 1.08 million years. *Journal of Asian Earth Sciences* 155, 174–179.

Ma, L., Sun, Y., Tada, R., Yan, Y., Chen, H., Lin, M., Nagashima, K., 2015. Provenance fluctuations of aeolian deposits on the Chinese Loess Plateau since the Miocene. *Aeolian Research* 18, 1–9.

Maher, B.A., Thompson, R., 1992. Paleoclimatic significance of the mineral magnetic record of the Chinese loess and paleosols. *Quaternary Research* 37, 155–170.

Maslin, M.A., Haug, G.H., Sarnthein, M., Tiedemann, R., Erlenkeuser, H., Stax, R., 1995. Northwest Pacific Site 882: the initiation of Northern Hemisphere glaciation. *Proceedings of the Ocean Drilling Program Scientific Results* 145, 315–333.

Miller, K.G., Wright, J.D., Browning, J.V., Kulpecz, A., Kominz, M., Naish, T.R., Cramer, B.S., Rosenthal, Y., Peltier, W.R., Sosdian, S., 2012. High tide of the warm Pliocene: implications of global sea level for Antarctic deglaciation. *Geology* 40, 407–410.

Moore, P.D., Webb, J.A., Collison, M.E., 1991. *Pollen Analysis*. Blackwell Scientific, Oxford.

Muller, R.A., MacDonald, G.J., 1997. Glacial cycles and astronomical forcing. *Science* 277, 215–218.

Naish, T., Powell, R., Levy, R., Wilson, G., Scherer, R., Talarico, F., Krissek, L., *et al*., 2009. Obliquity-paced Pliocene west Antarctic ice sheet oscillations. *Nature* 458, 322–328.

Nicholson, U., van der Es, B., Clift, P.D., Flecker, R., Macdonald, D.I.M., 2016. The sedimentary and tectonic evolution of the Amur River and North Sakhalin Basin: new evidence from seismic stratigraphy and Neogene–recent sediment budgets. *Basin Research* 28, 273–297.

Nowaczyk, N.R., Haltia, E.M., Ulbricht, D., Wennrich, V., Sauerbrey, M.A., Rosén, P., Vogel, H., Francke, A., Meyer-Jacob, C., Andreev, A.A., 2013. Chronology of Lake El'gygytgyn sediments—a combined magnetostratigraphic, palaeoclimatic and orbital tuning study based on multi-parameter analyses. *Climate of the Past* 9, 2413–2432.

Ogg, J.G., 2012. Geomagnetic polarity time scale. In: Gradstein, F.M., Ogg, J.G., Schmitz, M.D., Ogg, G.M. (Eds.), *The Geologic Time Scale*. Elsevier, Boston, pp. 85–113.

Palike, H., Frazier, J., Zachos, J.C., 2006. Extended orbitally forced palaeoclimatic records from the equatorial Atlantic Ceara Rise. *Quaternary Science Reviews* 25, 3138–3149.

Pavlyutkin, B.I., Petrenko, T.I., 2010. *Stratigraphy of Paleogene–Neogene Sediments in Primorye*. [In Russian.] Dalnauka, Vladivostok.

Pavlyutkin, B.I., 2015. The genus *Quercus* (Fagaceae) in the early Oligocene flora of Kraskino, Primorskii Region. *Paleontological Journal* 49, 668–676.

Prokopenko, A.A., Hinnov, L.A., Williams, D.F., Kuzmin, M.I., 2006. Orbital forcing of continental climate during the Pleistocene: a complete astronomically tuned climatic record from Lake Baikal, SE Siberia. *Quaternary Science Reviews* 25, 3431–3457.

Qi, F., Zhang, M., Lu, S., Bai, Y., Yang, W., 2015. *Quaternary Geology of Sanjiang Plain*. [In Chinese.] Geological Press, Beijing.

Qiang, X.K., Li, Z.X., Powell, C.M., Zheng, H.B., 2001. Magnetostratigraphic record of the late Miocene onset of the East Asian monsoon, and Pliocene uplift of northern Tibet. *Earth and Planetary Science Letters* 187, 83–93.

Qiu, S., Wan, E., Wang, P., 1988. Shoreline vicissitude of Lake Xingkai and discovery of ancient source of Songacha River. [In Chinese.] *Chinese Science Bulletin* 33, 937–940.

https://doi.org/10.1017/qua.2019.45 Published online by Cambridge University Press

Qiu, S.W., Wan, E.P., Li, F.H., Wang, P.F., 2007. Development of the plain in the north of the Xingkai Lake and formation of its wetlands. [In Chinese with English abstract.] *Wetland Science* 5, 153–158.

Qiu, S.W., Wang, X.K., Makhinov, A.N., Yan, B.X., Lian, y., Zhu, J.H., Zhang, F.L., Zhang, Z.Q., 2014. Summary of the paleodrainage pattern changes in the Northeast China Plain and its neighboring areas. [In Chinese with English abstract.] *Acta Geographica Sinica* 69, 1604–1614.

Raymo, M.E., Ruddiman, W.F., Backman, J., Clement, B.M., Martinson, D.G., 1989. Late Pliocene variation in Northern Hemisphere ice sheets and North Atlantic deep water circulation. *Paleoceanography* 4, 413–446.

Ren, G.Y., Zhang, L.S., 1998. A preliminary mapped summary of Holocene pollen data for northeast China. *Quaternary Science Reviews* 17, 669–688.

Ruddiman, W.F., Raymo, M.E., Martinson, D.G., Clement, B.M., Backman, J., 1989. Pleistocene evolution: Northern Hemisphere ice sheets and North Atlantic Ocean. *Paleoceanography* 4, 353–412.

Ruddiman, W.F., Raymo, M., McIntyre, A., 1986. Matuyama 41,000-year cycles: North Atlantic Ocean and northern hemisphere ice sheets. *Earth and Planetary Science Letters* 80, 117–129.

Shackleton, N.J., Berger, A., Peltier, W.R., 1990. An alternative astronomical calibration of the lower Pleistocene timescale based on ODP site 677. *Transactions of the Royal Society of Edinburgh: Earth Sciences* 81, 251–261.

Shen, J., Wang, S.M., Wang, Y., Qiang, X.K., Xiao, H.F., Xiao, X.Y., 2010. Uplift events of the Qinghai-Tibetan Plateau and environmental evolution of the southwest monsoon since 2.7 Ma, recorded in a long lake sediment core from Heqing, China. *Quaternary International* 218, 67–73.

Sun, W.W., Shen, J., Yu, S.Y., Long, H., Zhang, E.L., Liu, E.F., Chen, R., 2018. A lacustrine record of East Asian summer monsoon and atmospheric dust loading since the last interglaciation from Lake Xingkai, northeast China. *Quaternary Research* 89, 270–280.

Sun, X.J., Wang, P.X., 2005. How old is the Asian monsoon system? Palaeobotanical records from China. *Palaeogeography, Palaeoclimatology, Palaeoecology* 222, 181–222.

Sun, X.J., Weng, C.Y., 1992. Pollen records on the history of mixed conifer and hardwood forest in northeast China. [In Chinese with English abstract.] *Acta Botanica Sinica* 34, 394–401.

Sun, Y.B., An, Z.S., Clemens, S.C., Bloemendal, J., Vandenberghe, J., 2010. Seven million years of wind and precipitation variability on the Chinese Loess Plateau. *Earth and Planetary Science Letters* 297, 525–535.

Sun, Y.B., Clemens, S.C., An, Z.S., Yu, Z.W., 2006a. Astronomical timescale and palaeoclimatic implication of stacked 3.6-Myr monsoon records from the Chinese Loess Plateau. *Quaternary Science Reviews* 25, 33–48.

Sun, Y.B., Lu, H.Y., An, Z.S., 2000. Grain size distribution of quartz isolated from Chinese loess/paleosol. *Chinese Science Bulletin* 45, 2296–2298.

Sun, Y.B., Lu, H.Y., An, Z.S., 2006b. Grain size of loess, palaeosol and red clay deposits on the Chinese Loess Plateau: significance for understanding pedogenic alteration and palaeomonsoon evolution. *Palaeogeography Palaeoclimatology Palaeoecology* 241, 129–138.

Svenning, J.C., 2003. Deterministic Plio-Pleistocene extinctions in the European cool-temperate tree flora. *Ecology Letters* 6, 646–653.

Tan, N., Ramstein, G., Dumas, C., Contoux, C., Ladant, J.-B., Sepulchre, P., Zhang, Z.S., De Schepper, S., 2017. Exploring the MIS M2 glaciation occurring during a warm and high atmospheric CO_2 Pliocene background climate. *Earth and Planetary Science Letters* 472, 266–276.

Tian, J., Wang, P.X., Chen, R.H., Cheng, X.R., 2005. Quaternary upper ocean thermal gradient variations in the South China Sea: implications for East Asian monsoon climate. *Paleoceanography* 20, 4007–4014.

Tian, J., Wang, P.X., Cheng, X.R., Li, Q.Y., 2002. Astronomically tuned Plio–Pleistocene benthic $\delta^{18}O$ record from South China Sea and Atlantic–Pacific comparison. *Earth and Planetary Science Letters* 203, 1015–1029.

Tian, J., Zhao, Q.H., Wang, P.X., Li, Q.Y., Cheng, X.R., 2008. Astronomically modulated Neogene sediment records from the South China Sea. *Paleoceanography* 23, 3210–3229.

Torres, V., Hooghiemstra, H., Lourens, L., Tzedakis, P.C., 2013. Astronomical tuning of long pollen records reveals the dynamic history of montane biomes and lake levels in the tropical high Andes during the Quaternary. *Quaternary Science Reviews* 63, 59–72.

Utescher, T., Bondarenko, O.V., Mosbrugger, V., 2015. The Cenozoic cooling—continental signals from the Atlantic and Pacific side of Eurasia. *Earth and Planetary Science Letters* 415, 121–133.

Wan, S.M., Li, A.C., Clift, P.D., Stuut, J.-B.W., 2007. Development of the East Asian monsoon: mineralogical and sedimentologic records in the northern South China Sea since 20 Ma. *Palaeogeography, Palaeoclimatology, Palaeoecology* 254, 561–582.

Wang, P.X., Li, Q.Y., Tian, J., 2014a. Pleistocene paleoceanography of the South China Sea: progress over the past 20 years. *Marine Geology* 352, 381–396.

Wang, P.X., Wang, B., Cheng, H., Fasullo, J., Guo, Z.T., Kiefer, T., Liu, Z.Y., 2014b. The global monsoon across timescales: coherent variability of regional monsoons. *Climate of the Past* 10, 2007–2052.

Wang, P.X., Wang, B., Cheng, H., Fasullo, J., Guo, Z.T., Kiefer, T., Liu, Z.Y., 2017. The global monsoon across time scales: mechanisms and outstanding issues. *Earth-Science Reviews* 174, 84–121.

Wang, Y.X., Yang, J.D., Chen, J., Zhang, K.J., Rao, W.B., 2007. The Sr And Nd isotopic variations of the Chinese Loess Plateau during the past 7 Ma: implications for the East Asian winter monsoon and source areas of loess. *Palaeogeography Palaeoclimatology Palaeoecology* 249, 351–361.

[WCRP] World Climate Research Programme, 2009. *WCRP Implementation Plan 2010–2015*. WCRP, Geneva.

Xia, Y.M., 1988. Preliminary study on vegetational development and climatic changes in the Sanjiang Plain in the last 12,000 years. [In Chinese with English abstract.] *Scientia Geographica Sinica* 8, 240–249.

Xiao, J., Porter, S.C., An, Z.S., Kumai, H., Yoshikawa, S., 1995. Grain size of quartz as an indicator of winter monsoon strength on the loess plateau of central China during the last 130,000 yr. *Quaternary Research* 43, 22–29.

Xiong, S.F., Ding, Z.L., Jiang, W.Y., Yang, S.L., Liu, T.S., 2003. Initial intensification of East Asian winter monsoon at about 2.75 Ma as seen in the Chinese eolian loess-red clay deposit. *Geophysical Research Letters* 30, 1524–1527.

Yan, Y., Ma, L., Sun, Y.B., 2017. Tectonic and climatic controls on provenance changes of fine-grained dust on the Chinese Loess Plateau since the late Oligocene. *Geochimica et Cosmochimica Acta* 200, 110–122.

Yang, S.L., Ding, Z.L., 2010. Drastic climatic shift at ~2.8 Ma as recorded in eolian deposits of China and its implications for redefining the Pliocene–Pleistocene boundary. *Quaternary International* 219, 37–44.

Yi, L., Jian, Z.M., Liu, X.Y., Zhu, Y.H., Zhang, D.J., Wang, Z.F., Deng, C.L., 2018. Astronomical tuning and magnetostratigraphy of Neogene biogenic reefs in Xisha Islands, South China Sea. *Science Bulletin* 63, 564–573.

Yu, Z.W., Ding, Z.L., 1998. An automatic orbital tuning method for paleoclimate records. *Geophysical Research Letters* 25, 4525–4528.

Zeng, L., Lu, H.Y., Yi, S.W., Li, Y.X., Lv, A.Q., Zhang, W.C., Xu, Z.W., Wu, H.F., Feng, H., Cui, M.C., 2016. New magnetostratigraphic and pedostratigraphic investigations of loess deposits in north-east China and their implications for regional environmental change during the mid-Pleistocene climatic transition. *Journal of Quaternary Science* 31, 20–32.

Zeng, L., Lu, H.Y., Yi, S.W., Stevens, T., Xu, Z.W., Zhuo, H.X., Yu, K.F., Zhang, H.Z., 2017. Long-term Pleistocene aridification and possible linkage to high-latitude forcing: new evidence from grain size and magnetic susceptibility proxies from loess-paleosol record in northeastern China. *Catena* 154, 21–32.

Zhan, T., Zeng, F., Xie, Y., Yang, Y., Ge, J., Ma, Y., Chi, Y., Kang, C., Jiang, X., Yu, Z., Zhang, J., Li, E., Zhou, X., 2019. Magnetostratigraphic dating of a drill core from the Northeast Plain of China: implications for the evolution of Songnen paleo-Lake. [In Chinese with English abstract.] *Chinese Science Bulletin* 64, 1179–1190.

Zhang, J., Li, J.J., Guo, B.H., Ma, Z.H., Li, X.M., Ye, X.Y., Yu, H., *et al*., 2016. Magnetostratigraphic age and monsoonal evolution recorded by the thickest Quaternary loess deposit of the Lanzhou region, western Chinese Loess Plateau. *Quaternary Science Reviews* 139, 17–29.

Zhang, X., Guo, Y., Zeng, Z., Fu, Q., Pu, J., 2015. Dynamic evolution of the Mesozoic–Cenozoic basins in the northeastern China. [In Chinese with English abstract.] *Earth Science Frontiers* 22, 88–98.

Zhao, M.X., Wang, P.X., Tian, J., Li, J.R., 2009. Biogeochemistry and the carbon reservoir. In: Wang, P., Li, Q. (Eds.), *The South China Sea: Paleoceanography and Sedimentology*. Springer, Dordrecht, Netherlands, pp. 439–483.

Zijderveld, J.D.A., 1967. A. C. Demagnetization of rocks: analysis of results. In: Collinson, D.W., Creer, K.M., Runcorn, S.K. (Eds.), *Methods in Palaeomagnetism*. Elsevier, New York, pp. 254–286.

https://doi.org/10.1017/qua.2019.45 Published online by Cambridge University Press